Citrus vascular proteomics highlights the role of peroxidases and serine proteases during Huanglongbing disease progression

Jessica Y. Franco[1], Shree P. Thapa[1], Zhiqian Pang[2], Fatta B. Gurung[3], Thomas W.H. Liebrand[1], Danielle M Stevens[1], Veronica Ancona[3], Nian Wang[2], Gitta Coaker[1]

[1]Department of Plant Pathology, University of California, Davis, USA,

[2]Citrus Research and Education Center, University of Florida, Lake Alfred, USA,

[3]Citrus Center, Texas A&M University- Kingsville, Wescalo, Texas, USA,

*Corresponding author: Gitta Coaker (glcoaker@ucdavis.edu)

Running Title: Vascular proteomics in citrus during Huanglongbing disease

Abbreviations: HLB, huanglongbing; *C*Las, *Candidatus* Liberibacter asiaticus; ACP, Asian citrus psyllid; ABPP, activity-based protein profiling; PCA, principle component analysis.

Abstract:

Huanglongbing (HLB) is the most devastating and widespread citrus disease. All commercial citrus varieties are susceptible to the HLB-associated bacterium, *Candidatus* Liberibacter asiaticus (*C*Las), which resides in the phloem. The phloem is part of the plant vascular system and is involved in sugar transport. To investigate the plant response to *C*Las, we enriched for proteins surrounding the phloem in an HLB susceptible sweet orange variety, Washington navel (*Citrus sinensis* (L) Osbeck). Quantitative proteomics revealed global changes in the citrus proteome after *C*Las inoculation. Plant metabolism and translation were suppressed, while defense-related proteins including proteases and protease inhibitors were induced in the vasculature. Specific serine proteases were upregulated in Washington navel in the presence of *C*Las based on quantitative proteomics. Subsequent activity-based protein profiling revealed genotype-specific variation in serine protease activity in other *C. sinensis* sweet orange varieties. Plant peroxidases involved in extracellular ROS production or scavenging were induced in vascular enriched tissues based on quantitative proteomics. While peroxidase transcript accumulation was induced in *C*Las infected sweet orange varieties, peroxidase enzymatic activity varied between varieties, supporting the genotype-specific regulation of enzymatic activity. The observations in the current study highlight dynamic global reprogramming of the citrus vascular proteome and genotype-specific regulation of different enzyme classes in response to *C*Las infection. These results open an avenue for further investigation of diverse responses to HLB across different citrus genotypes.

46 **Introduction**

47 Currently, the citrus industry is facing a major threat from the bacterial vector-borne
48 disease huanglongbing (HLB), also known as citrus greening. The HLB-associated pathogen,
49 *Candidatus* Liberibacter asiaticus (*C*Las), is spread by *Diaphorina citri*, a hemipteran insect. All
50 commercial citrus varieties are susceptible to *C*Las and current interventions such as *D. citri*
51 control and infected tree removal have had little success in controlling the disease (1). Sweet
52 orange varieties (*Citrus sinensis*) exhibit the fastest decline, while lemon (*C. latifolia*),
53 mandarins (*C. reticulata*), and tangerines (*C. reticulata*) present delayed symptom progression
54 but ultimately succumb to HLB (2, 3). In the United States, HLB was first diagnosed in 2005 in
55 Florida and has since spread to Texas, Louisiana, South Carolina, Georgia and California (4). In
56 California, *C*Las positive citrus was detected in 2012 and there are currently 1,788 positive
57 plants identified by qPCR (5, 6). In Florida, it is estimated that 95% of mature trees in
58 commercial groves are infected, resulting in a loss of over 7.8 billion dollars in revenue and
59 7,500 jobs since 2007 (7). For decades, Florida has been the primary citrus producer in the
60 United States. However, due to losses from HLB, California is now the primary citrus producing
61 area (8).

62 Plant pathogens can be directly deposited into the vascular system (xylem or phloem) by
63 piercing sucking insects. *D. citri* deposits *C*Las into plant phloem sieve elements, where the
64 bacteria proliferate (9). The phloem is rich in sugars, amino acids, and proteins (10). *C*Las
65 infected leaf tissues exhibit increased deposition of callose, a beta 1-3 glucan, and accumulation
66 of starch that constricts symplastic transport, which contributes to symptom development (11,
67 12). HLB symptoms are characterized by yellowing of the shoots and leaves as well as hard,
68 misshapen, and bitter fruit (13, 14). Early detection efforts have been challenging to develop due

69 to the long latent period and the uneven distribution of *C*Las within its plant host (15). The
70 inability to culture *C*Las has hampered progress in studying the pathogen and its virulence
71 mechanisms.

72 One of the paramount mechanisms of bacterial pathogenesis is the presence of secretion
73 systems facilitating the translocation of proteins, or effectors, to the plant host (16). *C*Las
74 possesses the type I and general sec secretion system (17, 18). The sec pathway is critical for
75 virulence in other phloem-colonizing pathogens including mollicutes (*Ca.* Phytoplasma) (19).
76 Most *C*Las sec-dependent effectors (SDEs) were highly expressed *in planta*, indicating they are
77 important for pathogen proliferation (18, 20, 21). Transient expression of a conserved *C*Las
78 SDE, SDE1, induces cell death, starch accumulation, and callose deposition in *Nicotiana*
79 *benthamiana* (22). In citrus, SDE1 inhibits the activity of immune related proteases which may
80 serve as a strategy to dampen defense responses (23). Multiple secreted *C*Las proteins can
81 suppress immune responses (23–26). Upon pathogen perception, the production of reactive
82 oxygen species (ROS), including hydrogen peroxide, serve as an antimicrobial as well as a
83 secondary immune signal (27, 28). *C*Las peroxiredoxins, LasBCP and LasdPrx5, increased
84 oxidative stress tolerance in *Liberibacter crescens* (a culturable surrogate for *C*Las) by
85 suppressing H_2O_2 accumulation (24, 29). *C*Las encodes a salicylic acid hydroxylase that
86 degrades salicylic acid (SA), a plant defense hormone (26). Collectively, these data demonstrate
87 that *C*Las actively manipulates plant defense responses.

88 In order to understand the *C. sinensis* response to *C*Las, previous studies have
89 investigated dynamic changes during infection by microarray, RNAseq, and proteomics (30–32).
90 Microarray analyses revealed induction of genes associated with sugar metabolism, plant
91 defenses, phytohormones, and cell wall metabolism in infected leaf samples (33). Transcripts

92 encoding proteins involved in sugar and starch metabolism, stress responses, transport,
93 detoxification, and lipid metabolism were significantly upregulated during *C*Las infection, while
94 processes involved in photosynthesis were downregulated in mature leaf, stem, and root tissues
95 (30, 31, 34, 35). *C*Las induces plant defense responses in leaf tissue, including the transcription
96 of pathogenesis-related (PR) genes, chitinases, callose synthases, and defense-related WRKY
97 transcription factors (11, 31, 33, 35, 36). Consistent with these observations, infected *C. sinensis*
98 midveins exhibit callose and starch accumulation in the sieve tubes that lead to phloem plugging
99 and collapse (33, 34, 37). However, in roots, genes encoding callose hydrolases were induced
100 and callose synthases were repressed (35). These data illustrate that not all tissue types respond
101 ubiquitously and highlight tissue-specific responses during *C*Las infection.
102 Multiple studies have elucidated host responses intact leaf, root, and fruit samples(30,
103 31, 35, 36). However, *C*Las is limited to phloem sieve elements and there is a lack of proteomic
104 studies on vascular exudates. In this study, we performed comparative proteomic analyses to
105 investigate changes in the vascular proteome after *C*Las infection in the sweet orange variety
106 Washington Navel (*Citrus sinensis* (L) Osbeck). Our results highlight the accumulation of
107 peroxidases and proteases upon *C*Las infection, indicating the activation of plant defense
108 responses. Multiple citrus peroxidases were induced at the transcript and protein level during
109 infection across different citrus genotypes and environmental conditions. Serine protease activity
110 in leaf tissues also dynamically changed after *C*Las infection under greenhouse and field
111 conditions. This study advances our understanding of vascular changes and highlights the
112 important role of peroxidases and proteases in different citrus genetic backgrounds during *C*Las
113 infection.
114

115 Experimental Procedures

116 *Experimental Design and Statistical Rationale*

117 For vascular proteomics, eight Washington Naval trees grafted onto Carrizo rootstock were
118 grown in the UC Davis Contained Research Facility, a Biosafety level 3 greenhouse. Seven
119 months after grafting onto Carrizo rootstock, plants were graft-inoculated or mock-inoculated
120 with the *C*Las isolate, HHCA obtained from Hacienda Heights, California, USA. Plants were
121 grown in a completely randomized design, tested for *C*Las titers by qPCR monthly, and vascular
122 exudates were harvested ten months post graft-inoculation. Vascular exudates from four mock
123 and four *C*Las-graft inoculated Washington navel trees were extracted using the centrifugation
124 method (10). For mass spectrometry analyses, samples were blinded to the operator. To quantify
125 differentially changing proteins, label-free quantification using MaxQuant (v 1.5.1.0) was
126 performed. Protein identification search parameters included a decoy search database in addition
127 to a False Discovery Rate (FDR) of < 0.05. Statistical analyses were performed on four
128 individual trees per treatment (n=4). Differentially changing proteins were identified using a
129 two-sample student's t-test with an alpha-value of 0.05 for truncation.

130

131 *Plant Growth and Inoculation Conditions*

132 Washington Navel: Proteomic analyses were performed on citrus grown and maintained at the
133 University of California, Davis Contained Research Facility greenhouse. The greenhouse
134 temperature was maintained at 27°C. High pressure sodium lights were provided as
135 supplemental lighting for 16 hours. The greenhouse was covered with shade cloth (50% shade)
136 between mid-April and mid-October. Eight Washington navel (*Citrus sinensis* (L.) Osbeck) buds

137 were grafted onto Carrizo rootstock using the inverted T budding method. After seven months,
138 four Washington navel scions were mock or *C*Las graft-inoculated on February 2014. Samples
139 were harvested 10 months post-graft inoculation and tested for *C*Las presence by qPCR each
140 month. A random sampling of 6-8 leaves was taken from each tree and pooled for DNA
141 extraction. DNA was extracted using the Qiagen MagAttract plant DNA extraction kit (Qiagen,
142 Valencia, CA, USA). *C*Las presence was detected by qPCR using the USDA-APHIS-PPQ
143 protocol (38). *C*Las primers amplifying the 16s rDNA (HLBas/HLBr) were used for *C*Las
144 detection. The citrus cytochrome oxidase (COXf/r) primers and probe were used as an internal
145 control (38). All primers, gene names, and accession numbers are provided in Supplementary
146 Table S1.

147 Hamlin sweet orange: Hamlin sweet oranges (*Citrus sinensis* (L) Osbeck) were grown in the
148 greenhouse at 25°C. Trees were exposed to *C*Las positive *D. citri* for 2 months. Psyllids were
149 removed and plants were transferred to a psyllid-free greenhouse and sampled one year after
150 *C*Las transmission. *C*Las detection was performed using ethidium bromide monoazide (EMA)-
151 qPCR using primers that amplify the β-operon (39). Samples were collected from uninfected and
152 symptomatic Hamlin sweet orange, flash frozen, and sent to the Contained Research Facility on
153 dry ice for further processing.

154 N-33: Mature N-33 (*Citrus sinensis* (L) Osbeck) trees were grown in a commercial orchard in
155 Donna, TX. Leaf samples from symptomatic trees grown in the field and uninfected trees from
156 an adjacent screenhouse were collected and flash frozen in liquid nitrogen. *C*Las detection was
157 performed using qPCR with primers that amplify the 16s rDNA (HLBas/HLBr) and the *C.*
158 *sinensis* GAPDH gene was used as an internal control. Samples were sent on dry ice to the
159 Contained Research Facility at the University of California, Davis for further processing.

160

161 *Protein extraction for Mass Spectrometry*

162 Citrus vascular exudates were enriched by centrifugation (10). Stems were collected from 17-
163 month-old greenhouse plants and the outer bark was manually removed. The inner part of the
164 bark was briefly rinsed with deionized water and dried with Kimwipes. The bark was cut into 1
165 cm pieces using a razor blade and placed into a 0.65 mL Eppendorf tube with a small hole in the
166 bottom. This tube was then placed into a 1.7 mL Eppendorf collection tube and centrifuged at
167 12,000 x g for 15 min at 25°C. Vascular extracts were flash frozen and stored at -80°C. Samples
168 were resuspended in 2x Laemmli buffer and quantified for protein concentration using the Pierce
169 660nm Protein Assay Reagent (Thermo Fisher Scientific).

170 A total of 85 µg of protein per sample was subjected to one-dimensional SDS-PAGE using an 8-
171 16% precise protein gradient gel (Thermo Fisher Scientific). Proteins were separated for 1 cm in
172 the resolving gel and the entire lane was excised and cut into equal pieces. In-gel reduction was
173 performed by adding 10 mM dithiothreitol in 50 mM ammonium bicarbonate for 30 min at 56°C.
174 Alkylation was performed by adding 55 mM iodoacetamide in 50 mM of ammonium bicarbonate
175 for 20 min in the dark with shaking at room temperature. In-gel tryptic digestion was performed
176 using 300 ng of trypsin in 50 mM ammonium bicarbonate (40). The digested peptides were dried
177 in a vacuum concentrator and then solubilized in 120 µL of 2% acetonitrile, 0.1% trifluoroacetic
178 acid for LC-MS/MS analysis.

179

180 *LC-MS/MS*

181 Peptides were submitted to the Genomics Center Proteomics Core at the University of California,
182 Davis for liquid chromatography tandem mass spectrometry (LC)-MS/MS. Peptides were
183 analyzed by MS as described previously (23). The LC-MS/MS system configuration consisted of
184 a CTC Pal autosampler (LEAP Technologies) and Paradigm HPLC device (Michrom
185 BioResources) coupled to a QExactive hybrid quadrupole Orbitrap mass spectrometer (Thermo
186 Fisher Scientific) with a CaptiveSpray ionization source (Michrom BioResources). Peptides were
187 reconstituted in 2% acetonitrile and 0.1% formic acid and were washed on a Michrom C18 trap
188 then were eluted and separated on a Michrom Magic C18AQ (200 μm × 150 mm) capillary
189 reverse-phase column at a flow rate of 3 μL/min. A 120 min gradient was applied with a 2% to
190 35% B (100% acetonitrile) for 100 min, a 35% B to 80% B for 7 min and 80% B for 2 min. Then
191 a decrease of 80% to 5% B in 1 min followed by 98% A (0.1% formic acid) for 10 min. The
192 QExactive was operated in Data-Dependent Acquisition (DDA) mode with a top-15 method.
193 Spray voltage was set to 2.2 kV. The scan range was set to 350–1600 m/z, the maximum
194 injection time was 30 ms and automatic gain control was set to 1×10^6. Precursor resolution was
195 set to 70,000. For MS/MS, the maximum injection time was 50 ms, the isolation window was 1.6
196 m/z, the scan range 200–2000 m/z, automatic gain control was set to 5 × 104 and normalized
197 collision energy was 27%. The dynamic exclusion window was set to 15 s and fragment product
198 resolution was 17,500. An intensity threshold of 1 × 104 was applied and the underfill ratio was
199 1%.

200

201 *Peptide identification, analyses and quantification*

202 The raw MS/MS data files were imported into MaxQuant v1.5.1.0 for label-free intensity-based
203 quantification (41). The database search engine Andromeda (42) was used to search MS/MS

204 spectra against the *C. clementina* (v1.0) and *C. sinensis* (v1.0) databases downloaded from
205 Phytozome (43) and the *Candidatus* Liberibacter asiaticus (CLas) proteome database (44)
206 downloaded from Uniprot with a tolerance level of 20 ppm for the first search and 6 ppm for the
207 main search. Trypsin/P was set as the enzyme and two missed cleavages were allowed. Protein
208 N-terminal acetylation and Methionine oxidation were set as variable modifications. The
209 maximum number of modifications per peptide was set as five and the predefined contaminants
210 from MaxQuant were included in the search database. The 'match between runs' feature was
211 checked with a match time window of 0.7 min and an alignment time window of 20 min. The
212 FDR for protein level and peptide spectrum match was set to 1%. The minimum peptide length
213 was 6, minimum razor was changed to 0, and minimum unique peptides was set to 1. The
214 minimum ratio count for protein quantification was set to 2. The other MaxQuant settings were
215 default. The total peptide intensities for each replicate were summed and a normalization factor
216 was calculated for each sample (41). This normalization factor was applied based on the least
217 overall proteome change. Peptide ratios between samples were then calculated to obtain a pair-
218 wise protein ratio matrix between samples, which was subsequently used to rescale the
219 cumulative intensity in each sample and provides the label-free intensity (LFQ) value (41).
220 Parameters used in MaxQuant can be found in Supplementary Table S2. The MaxQuant output
221 file "Protein Groups" was imported into Perseus 1.5.5.3 (45). Contaminants, reverse hits, and
222 proteins identified only by modified peptides were excluded in subsequent analysis. The LFQ
223 intensities were log2-transformed. Proteins not consistently identified in at least two out of the
224 four replicates in at least one group were discarded. Missing values were imputed with values
225 from a normal distribution of the obtained intensities using default settings (width 0.5, downshift
226 1.8). Differentially changing proteins were identified using a two-tailed Student's t-test, $p<0.05$,

227 with a permutation-based FDR of 0.05 to correct for multiple testing. The mass spectrometry
228 proteomics data have been deposited to the ProteomeXchange Consortium via the PRIDE (46)
229 partner repository with the dataset identifier PXD017480.

230

231 *Comparative analyses of proteomics data*

232 Initial data visualization was performed using Perseus (Version 1.5.5.3) software. The heatmap
233 was generated by hierarchical clusters for both individual protein expression and replication was
234 performed using Euclidean distance (47). Linkage was calculated using preprocessed k-means
235 with 300 clusters, 10 maximal iterations, and 1 restart. Principle component analyses was
236 performed using untransformed label-free values.

237

238 *Comparison of vascular proteomic studies*

239 Homologs of citrus proteins identified by mass spectrometry were identified using BLAST
240 analyses (version 2.2.18) against *Arabidopsis thaliana* (48, 49) and *Cucumis sativus* (50) phloem
241 proteins with an E-value of 1e−10 required for protein identification. The Venn diagram was
242 generated using the vennueler R package (51).

243 Gene ontology analyses were performed by using Phytozome (43). All identified protein groups
244 were used as background. Gene ontology enrichment for differentially changing proteins using
245 the Bonferroni test was used for correction with an alpha-value of 0.05. The p-values and gene
246 ontology terms can be found in Supplementary Tables S3-S6. A custom R script was designed to
247 filter redundant GO Terms and plotted in respect to the number of proteins which are

248 differentially regulated (Github: DanielleMStevens/Franco_2020_Proteomics_Paper) (47, 52).
249 Raw data and code can be found in the above repository.

250

251 *Phylogenetic analyses*

252 A total of 134 serine protease and 84 peroxidase sequences were obtained from Phytozome using
253 the *C. clementina* v1.0 and *C. sinensis* v1.0 databases (43, 53). Peroxidases were identified using
254 the RedOxiBase Database (http://peroxibase.toulouse.inra.fr/) and the pFAM domain PF00141.
255 Serine proteases were identified using the MEROPs peptidase database
256 (https://www.ebi.ac.uk/merops/index.shtml). Multiple sequence alignments were performed with
257 PRANK (54). A maximum likelihood approach was used to reconstruct phylogenetic trees using
258 RAxML (55). Bootstrapping was performed with 1,000 replicates. The resulting phylogenetic
259 trees were visualized using FigTree (version 1.4.3) (56).

260

261 *Activity Based Protein profiling (ABPP)*

262 Leaves from the *C. sinensis* N-33 and Hamlin varieties (n =4 trees) were ground in Tris-HCl pH
263 8.0 solution. The supernatant was collected and centrifuged at 5,000 x g for 10 min. Citrus
264 extracts were quantified using the Pierce 660 Protein assay kit (ThermoFisher Scientific). The
265 serine protease inhibitor cocktail (50 μM chymotrypsin, 50 μM PMSF, 50 μM of 3,4-
266 dichloroisocoumarin) was pre-incubated for 30 min prior to the addition of the ActivX TAMRA
267 fluorophosphonate (FP) serine hydrolase probe (ThermoFisher Scientific). For the no probe
268 control, 1 μL of dimethyl sulfoxide (DMSO) was added. The serine hydrolase FP probe was
269 added at a final concentration of 2 μM. Serine proteases were labeled for one hour, labeling

270 stopped by adding 2X Laemmli buffer, and the sample incubated at 95℃ for 5 min. Labeled
271 proteins were run on an 8-16% precise Tris-Glycine SDS page gel (ThermoFisher Scientific).
272 Serine protease activity was visualized by in-gel fluorescence using the Typhoon 8600 variable
273 mode Imager (Molecular Dynamics Inc, CA, USA). Significant differences in serine protease
274 activity were detected with a two-tailed unpaired Student's t-test alpha-value of 0.05.

275

276 *Peroxidase gene expression using RT-qPCR*

277 Hamlin sweet orange: Total RNA was extracted with the RNeasy Plant Mini Kit (Qiagen) and
278 treated with DNase I (Promega). First-strand cDNA was synthesized from purified RNA with
279 ImProm-II™ Reverse Transcription System (Promega) and diluted 10 times for RT-qPCR to
280 detect related genes with specific primers. Quantitative reverse transcription PCR reactions used
281 the 2xKiCqStart® SYBR® Green qPCR ReadyMix™ (Sigma-Aldrich). PCR consisted of an
282 initial activation step at 95°C for 3 min, followed by 40 cycles of 95°C for 15 s and 60°C for 40
283 s. All cDNA samples were run in triplicate. The *C. sinensis* GAPDH gene (XM_006476919.3)
284 was used to normalize the expression of each target gene and quantification was performed using
285 the ΔΔCt method. Significant differences (n=4) were detected with a two-tailed unpaired
286 Student's t-test.

287

288 N-33 sweet orange variety: Total RNA was extracted using a Trizol (Invitrogen, USA)-based
289 method and treated with DNase I (DNase Max Kit (50), QIAGEN). Quantitative reverse
290 transcription PCR reactions used Power SYBR™ Green RNA-to C_T™ 1-step kit (Applied
291 Biosystems-Thermo Fisher Scientific, USA). Thermocycling began with a Hold Stage (first step
292 at 48 °C for 30 s, second step 95 °C for 10 min), followed by a PCR stage (first step at 95°C for

293 15 s, second step 55 °C for 1 min over 40 cycles) in a thermal cycler (Applied Biosystems-
294 QuanStudio 3, Thermo Fisher Scientific, USA). The *C. sinensis* GAPDH gene
295 (XM_006476919.3) was used to normalize the expression of each target gene and quantification
296 was performed using the ΔΔCt method. Significant differences (n=3) were detected with a two-
297 tailed unpaired Student's t-test.
298
299 *Peroxidase activity*

300 Peroxidase activity was tested using a previously described protocol (57). Briefly, citrus
301 leaf punches (4 mm diameter) were excised and washed for 1 hr in 1x MS solution with
302 agitation. Each leaf disk was then transferred to a 96 well-microplate containing 50 µL of 1x MS
303 solution. Leaf disks were incubated for 20 h at 25°C with agitation. To observe peroxidase
304 accumulation, leaf disks were removed and 50 µL of 1mg/mL of 5-aminosalicylic acid, pH 6.0,
305 with 0.01% hydrogen peroxide was added and incubated for 1-3 min. The reaction was stopped
306 by adding 20 µM of 2 N NaOH. Optical density readings (OD_{600}) were measured using a
307 spectrophotometer. Uninfected samples were set to 100% peroxidase activity and changes in
308 peroxidase activity were calculated based on the ratio of OD_{600} readings (Infected/Uninfected).
309 Significant differences in peroxidase activity were detected with a two-tailed unpaired Student's
310 t-test.
311

312 **Results**

313 ***C*Las induces global changes in the citrus vascular proteome**

314 In order to investigate changes occurring in citrus tissues infected with *C*Las, we isolated
315 protein from bark samples ten months post-inoculation and performed proteomics analyses. The

316 sweet orange cultivar Washington navel (*Citrus sinensis* (L) Osbeck), which is susceptible to
317 HLB, was graft inoculated or mock inoculated with *C*Las positive budwood. At 10 months post-
318 inoculation, *C*Las inoculated navels exhibited severe HLB disease symptoms and detectable
319 *C*Las titers using qPCR (Supplementary Table S7). Total extracted proteins were subjected to
320 tandem mass spectrometry (LC-MS/MS) and MS1 quantification using MaxQuant (41). To
321 increase total protein identifications, the protein database included the *C. sinensis* and *C.*
322 *clementina* assembled genomes (53, 58). A total of 1,354 citrus proteins were identified using
323 MS1 quantification for infected and uninfected samples (Supplementary Table 8, Figure 1A).
324 Uninfected samples had an average of 1259 protein identifications and infected samples had an
325 average of 1152 protein identifications across all four biological replicates (trees). 329 (24%)
326 proteins were significantly upregulated and 363 (27%) proteins were downregulated in infected
327 samples (Supplementary Table 9 and 10, respectively). Hierarchical clustering based on
328 Euclidean distance revealed that samples clustered according to treatment (Fig. 1A) (45).
329 Similarly, principle component analyses (PCA) differentiated biological samples based on their
330 treatment (Fig. 1B.). Taken together, these data indicate that *C*Las infection induces global and
331 reproducible changes in vascular protein expression patterns (Fig 1A-B).
332 Isolation of pure phloem proteins is extremely difficult and can only be obtained using
333 microneedle puncture or the stylet of a phloem-feeding insect (59, 60). To increase phloem
334 yields, EDTA-facilitated exudation and centrifugation are commonly used (10). However, these
335 approaches are not amenable to citrus exhibiting HLB symptoms due to decreased phloem
336 transport. Therefore, we centrifuged the outer bark to extract vascular exudates and enrich for
337 phloem proteins. To ascertain if we enriched for phloem proteins, we compared the overlap in
338 protein identifications between our study with studies performed in *Cucumis sativus* and

339 *Arabidopsis* (48–50). Citrus homologs for 62% and 64% of the *Arabidopsis* and *Cucumis*
340 *sativus* proteins were identified, respectively (Fig. 1C.). Although these plants represent diverse
341 families (Rutaceae, Brassicaceae and Cucurbitaceae), many of the identified proteins overlapped.
342 These results indicate that vascular proteins were successfully extracted from citrus and identify
343 universal vascular proteins between diverse plant species.

344 To gain insight on the biological and molecular functions altered by *C*Las infection, we
345 performed gene ontology analyses using Phytozome (43). Processes involved in plant growth
346 and development including metabolism, translation and biosynthetic processes were inhibited
347 after *C*Las infection (Fig. 2). For example, many ribosomal proteins and translation elongation
348 factors were downregulated during infection. Proteins involved in glycolysis, such as pyruvate
349 kinases (orange1.1g036921m, orange1.1g010627m, Ciclev10031317m, orange1.1g010449m)
350 were significantly repressed during infection (Supplementary Table 10). In contrast, proteins
351 involved in pathogen perception were upregulated in infected samples. We identified multiple
352 proteins with receptor-like kinase or receptor-like protein domain architecture that were
353 upregulated during infection, including the receptor-like kinase, Ciclev10030933m, and the
354 LysM domain protein orange1.1g018290m (Supplementary Table 9). Proteins with this domain
355 architecture are frequently implicated in pathogen perception (27, 28, 61). Multiple peroxidases
356 and proteases were more abundant in *C*Las infected samples (Fig 2A, 2B). Both peroxidases and
357 proteases have been established as key components in development and plant defense responses
358 (62–65) . Taken together these results implicate the tradeoff between growth and defense during
359 *C*Las infection.
360
361

362 **Peroxidase transcript and protein abundance increases during *C*Las infection**

363 In order to gain a greater understanding of citrus peroxidases, we identified and classified
364 peroxidases in the *C. sinensis* and *C. clementina* genomes. In plants, the heme peroxidase-
365 catalase superfamily (PCATS) can be further classified into three distinct classes with plants
366 possessing only class I and class III peroxidases (66). Both class I and class III peroxidases have
367 been implicated to function in growth, development, and immunity (67). Class I peroxidases
368 encompass intracellular enzymes such as ascorbate peroxidases and catalases. Class III
369 peroxidases are a large family consisting of extracellular or vacuolar localized enzymes. Class III
370 peroxidases can regulate H_2O_2 abundance, oxidation of toxic substrates, and defense responses
371 (65, 68, 69). Due to redundancy, studies to identify the *in planta* role of most peroxidases
372 remains elusive (69). Using PeroxiBase, 80 peroxidases (13 class I, 67 class III) were identified
373 in *C. sinensis.* For phylogenetic analyses, an additional 4 peroxidases (2 class I, 2 class III)
374 identified from *C. clementina* were included (67) (Fig 3). Maximum-likelihood phylogenetic
375 analyses of these peroxidases were performed using RAxML (55). The identified ascorbate
376 peroxidases cluster appropriately within the class I clade (Fig 3). In the vascular proteome, 22
377 peroxidases were identified and 10 were upregulated during *C*Las infection (3 class I and 7 class
378 III) (Supplemental Figure 1, Supplementary Table 11). Taken together, these data highlight the
379 abundance of peroxidases in *C. sinensis* and reveal an overall increase in abundance of specific
380 members upon *C*Las infection.

381 The abundance of specific enzyme classes does not always correlate with their activity.
382 To test peroxidase protein accumulation and enzymatic activity during *C*Las infection, we
383 examined the *C. sinensis* Hamlin sweet orange variety, which is the most widely grown in
384 Florida for early harvest (70). Healthy and symptomatic leaf tissue from Hamlin oranges were

385 sampled one-year after *C*Las transmission by *D. citri* (Fig 4A). To test peroxidase gene
386 expression in Hamlin, qPCR was performed on seven peroxidase genes that were previously
387 identified as induced in our proteomics analyses. Four Hamlin peroxidases were induced in
388 infected samples and three were expressed at the same level in infected and uninfected samples
389 by qPCR (Fig 4B). We investigated peroxidase activity during *C*Las infection using a
390 microplate-based assay to quantify the basal levels of the reactive oxygen species, H_2O_2 (57).
391 Overall peroxidase activity decreased in infected Hamlin samples (Fig 4C). The disconnect
392 between peroxidase mRNA expression and enzymatic activity may be due to *C*Las manipulation
393 of enzymatic activity or opposing roles of specific enzymes.
394 N-33 is a Navel orange variety frequently grown in Texas (71). To test peroxidase
395 accumulation under field conditions and with another *C. sinensis* variety, mature N-33 plants
396 were sampled for peroxidase accumulation by qPCR and enzymatic activity. Symptomatic leaves
397 and healthy leaves from an adjacent screenhouse were collected. To validate *C*Las infection,
398 qPCR was performed on seven peroxidases identified in our proteomics analyses as described
399 above (Fig 4D). The transcript abundance of all analyzed peroxidases in N-33 was higher in
400 infected samples, with five demonstrating a statistically significant increase (Fig 4E).
401 Furthermore, peroxidase enzymatic activity was significantly higher in N-33 infected leaf tissue
402 (Fig 4F). These data highlight the responsiveness of individual peroxidases during *C*Las
403 infection and indicate that the response to *C*Las can be influenced by plant genotype and/or
404 environmental effects.
405
406
407

408 **Diverse proteases and protease inhibitors dynamically change during infection**

409 Proteolysis is an enriched biological process and molecular function in the mass
410 spectrometry quantification of vascular proteins from *C*Las-infected citrus (Fig 2A, Fig 2B).
411 Plant proteases are divided into seven classes: serine, aspartic, cysteine, asparagine, threonine,
412 glutamate, and metalloproteases (72). Proteases degrade misfolded and toxic proteins. This
413 function plays important regulatory roles in development, reproduction and immunity (73). To
414 regulate proteolysis, protease inhibitors target their corresponding proteases. In the proteome of
415 vascular exudates, both proteases and protease inhibitors were present and dynamically
416 responded to infection. A total of 22 serine, 15 aspartic, 12 cysteine and 2 metalloproteases were
417 identified (Fig 5A).

418 Serine proteases are among the largest protease class in plants encompassing over 200
419 members and are divided into 14 families (73, 74). The classification of serine proteases depends
420 on the catalytic mechanism and common ancestry (75). Members of the subtilases (S8), serine
421 carboxypeptidases (S10), and lysosomal Pro-x carboxypeptidases (S28) families of serine
422 proteases were identified in our proteomics analyses (Fig 5F, Supplementary Fig. 2).
423 Phylogenetic analyses of 67 S8, 48 S10, and 19 S28 serine proteases from *C. sinensis* and *C.*
424 *clementina* were performed (72). . Differentially accumulating proteases did not cluster
425 phylogenetically (Supplementary Fig. 2). S10 proteases generally increased during infection
426 except for one member, orange1.1g010508 (Fig 5F). Subtilisin and serine carboxypeptidases
427 comprise the largest serine protease class, have had prior implications in plant immunity, and are
428 directly inhibited by diverse pathogen classes (73–77). These results indicate that the S8, S10,
429 and S28serine proteases families are most responsive to *C*Las infection.

430 In general, protease inhibitors inhibit a single catalytic class of proteases, however, some
431 families can inhibit multiple protease classes (78). Cystatins are simple protease inhibitors that
432 target papain like cysteine proteases (PLCPs) and metacaspase-like cysteine proteases. Cystatins
433 have dual roles as defense proteins and regulators of PLCP protein turnover (79). In this
434 proteomic study, five cystatins were identified, but only one decreased in abundance during
435 infection (Fig 5A-B). Diverse serine protease inhibitors were identified in the vasculature (Fig
436 5A-B). Two potato type I (Pin1) serine protease inhibitors were identified, but not changing
437 during *C*Las infection (Supplementary Table 12). Kunitz trypsin inhibitors and SERine Protease
438 INhibitors (SERPINs) are the most extensively studied and can inhibit diverse protease classes
439 (78, 80). Kunitz trypsin inhibitors are capable of binding to serine, cysteine and aspartic
440 proteases (78). SERPINs are active serine protease inhibitors, but can also inhibit some cysteine
441 proteases (78). Nine Kunitz trypsin inhibitors were identified (five induced) and two SERPINs
442 were identified (one induced) (Fig 5A, B). Kunitz trypsin inhibitors and SERPINs have been
443 demonstrated to have inhibitory effects against pathogens and insects (78). Our proteomics
444 analyses indicate protease activity is tightly regulated during *C*Las infection.
445

446 **Serine protease activity dynamically changes during *C*Las infection**

447 To quantify the activity of serine proteases during *C*Las infection, activity-based protein
448 profiling (ABPP) was performed. ABPP enables detection of active proteases with probes
449 specific to protease class (81, 82). For ABPP, we used the Hamlin and N-33 varieties grown in
450 the Florida greenhouse and Texas field, respectively. Proteases from four uninfected and four
451 infected samples were extracted from leaf tissue and subjected to ABPP (Fig 6A). A no probe
452 control was included to confirm probe binding to active proteases. Due to a lack of an effective

453 broad-spectrum serine protease inhibitor, an inhibitor cocktail containing phenylmethylsulphonyl
454 fluoride (PMSF), 3,4-dichloroisocoumarine and chymostatin was used to verify labeling
455 specificity. The inhibitor cocktail was added 30 min prior to the addition of the probe to
456 inactivate serine proteases. Serine protease activity is demonstrated by the presence of a band
457 detected by fluorescence imaging. Active serine protease bands were reduced in the presence of
458 the protease inhibitor cocktail, indicating that ABPP was able to specifically detect serine
459 protease activity (Fig 6B, D).

460 In Hamlin orange, three distinct protease signals changed during *C*Las infection (Fig 6B).
461 The intensity of bands 1 (~110 kD) and 2 (~100 kD) increased during infection and
462 quantification of the fluorescent signal across four biological replicates demonstrated this
463 increase in activity as statistically significant (Fig 6C). In contrast, band 3 (~30 kD) displayed a
464 significant decrease in protease activity during *C*Las infection. In N-33, bands 1-3 followed the
465 same trend (Fig 6D, E). Two additional groups of active serine protease bands were observed in
466 N-33 (Fig 6D). Due to the inability to resolve individual active serine protease bands, the
467 average signal was summed in the two different aggregates (bands 4 and 5). Bands 4 and 5
468 exhibited decreased activity (~40kD) (Fig 6E). These experiments demonstrate the induction and
469 activation of specific serine proteases during *C*Las infection is conserved across diverse
470 environmental conditions and sweet orange varieties. The decreased activity of specific serine
471 proteases during *C*Las infection may be due to the induction of plant serine protease inhibitors or
472 direct suppression by *C*Las.
473
474
475

476 **Discussion:**

477 HLB has caused billions of dollars in economic losses worldwide and continues to
478 threaten the United States citrus industry. To curb HLB losses, a detailed understanding of the
479 mechanisms of disease is essential to develop comprehensive disease management strategies.
480 Various -omics approaches have identified molecular pathways altered during *C*Las infection in
481 leaf, root, stem, and fruit tissues providing a heightened understanding of the responses in
482 diverse tissue types (31, 35, 83–85). For example, proteomics coupled with nutrient profiling
483 demonstrated that *C*Las infection reduces Ca^{+2}, Mg^{+2}, Fe^{+2}, Mn^{+4}, Zn^{+2} and Cu^{+} in grapefruit
484 leaves (86). Consistent with these observations, diseased plants supplemented with a cocktail of
485 Ca and Zn resulted in an increase in fruit production (87). However, these studies did not directly
486 address responses within the phloem, the niche where *C*Las resides and propagates. In this study,
487 we quantified proteins in vascular enriched samples to gain a greater understanding of proteomic
488 changes where *C*Las resides.

489 In Washington navel, we revealed global changes occur in vascular tissue, with 51% of
490 the total proteome dynamically changing during *C*Las infection. Upon pathogen perception,
491 cellular resources, which would otherwise be utilized in growth-related processes, are redirected
492 towards defense responses; this is known as the growth-defense tradeoff (88). In this study, we
493 observed evidence for this tradeoff during *C*Las infection, with defense associated proteins
494 induced in infected samples and processes involved in general housekeeping significantly
495 enriched in uninfected samples. In a parallel study on Washington navel leaf tissue, processes
496 involved in photosynthesis were downregulated while defense related processes were
497 significantly upregulated in *C*Las infected samples (83). These data indicate that the growth-
498 defense tradeoff also occurs in response to vascular pathogens. Washington navel is susceptible

499 to HLB, but clearly responded to *C*Las infection. It is unclear if HLB symptomology is due to a
500 lack of early and robust plant defense, or a result of a slower prolonged autoimmune response, or
501 possibly a combination of the two.

502 Reactive oxygen species (ROS) such as superoxide radicals, hydrogen peroxide and
503 singlet oxygen play a central role in plant pathogen defense (89). ROS is produced at the plasma
504 membrane by NAD(P)H oxidases and apoplastic peroxidases (89). ROS also accumulates in
505 different organelles including the chloroplast, mitochondria, and peroxisomes (89). Despite the
506 importance of ROS for defense signaling, an overabundance is cytotoxic and therefore requires
507 tight control (89). In melon, redox-related proteins, including peroxidases, are phloem localized
508 and induced during viral infection (48, 90). In this study, the transcription of seven peroxidases
509 that were more abundant in proteomics analyses, were also upregulated in infected samples from
510 different locations and citrus varieties. ROS regulating enzymes are upregulated at the protein
511 level in grapefruit after *C*Las infection (86, 91). Citrus undergoing thermotherapy to treat HLB
512 exhibited increased peroxidase accumulation (92). Additionally, bioinformatic analyses
513 comparing four RNA-seq studies on HLB illustrated that tolerance is linked with the induction of
514 redox-related genes involved in both young and mature leaf tissues (93). These studies indicate
515 the importance of regulating the opposing roles of redox during CLas infection.

516 Plant proteases are involved in pathogen perception, defense priming, signaling, and
517 programmed cell death (77). To ensure tight control of protease activity, plants evolved protease
518 inhibitors that fine-tune protease activity. Protease inhibitors can also inhibit digestive proteases
519 from herbaceous insects and target pathogens (60, 78, 94, 95). Multiple classes of proteases and
520 protease inhibitors are found in the vasculature of diverse plant species (32, 94–98). In
521 *Arabidopsis,* tomato, and maize, papain-like cysteine proteases (PLCPs) positively regulate

522 immunity and defense hormone accumulation (77, 99, 100). In citrus, PLCPs are localized in
523 phloem-enriched tissue, immune related, and targeted by the conserved *C*Las effector, SDE1
524 (23). In this study, proteases and their inhibitors were the largest class of dynamically changing
525 proteins during *C*Las infection. In Hamlin and N-33 sweet orange varieties, we observed
526 activation and inhibition of specific citrus serine proteases, suggesting citrus fine-tunes protease
527 enzymatic activity during *C*Las infection. Genotype specific effects were also observed, with
528 specific groups of serine proteases inhibited in the N-33 variety, but not in the Hamlin variety.
529 Whether this inhibition is due to the endogenous activity of plant protease inhibitors or *C*Las
530 inhibition of citrus proteases needs further investigation.

531 Comparative analyses of different citrus genotypes are beginning to reveal the
532 importance of genotype specific responses. RNA-seq analyses between the more HLB-tolerant
533 rough lemon (*Citrus jambhiri*) and susceptible sweet orange (*C. sinensis* (L) Osbeck)
534 demonstrated that the expression amplitude of defense related genes was much higher in the
535 HLB tolerant-rough lemon than HLB-susceptible sweet orange (85). In two susceptible
536 genotypes, Lisbon lemon and Washington navel, the root metabolome and microbiome differed
537 in response to *C*Las. (101). However, both genotypes exhibited a reduction of sugars, the amino
538 acids proline and asparagine, and in some metabolites (101). These important findings are not
539 entirely unexpected as sweet oranges and lemons are different species and were derived from
540 different admixtures (102). In this study, we observed differences in peroxidase and serine
541 enzymatic activity in two sweet orange varieties, Hamlin and N-33 (101). This study reveals
542 even closely related genotypes within the same citrus species exhibit variations in their responses
543 to *C*Las. Future studies investigating diversity of citrus responses to HLB across different citrus

544 genotypes, *C*Las isolates, and environmental conditions will provide a comprehensive
545 understanding of disease development.
546

547 **Acknowledgements**

548 This research was supported by a USDA National Institute of Food and Agriculture grant #2016-
549 70016-24833 to G.C., V.A., and N.W and grant # 2019-70016-29796 awarded to G.C., and N.W.
550 Additional support was provided by the Citrus Research Board (CRB) project 5200-157. J.Y.F
551 was supported by the USDA National Institute of Food and Agriculture grant #2017-678011-
552 26039. T.W.H.L. was supported by a Rubicon grant of the Netherlands Organization for
553 Scientific Research (NWO).
554

555 **Author Contributions**

556 G.C. and J.YF. conceived and designed the study; J.Y.F, S.P.T., Z.P, F.B.G. and performed the
557 experiments. S.P.T., T.W.H.L and D.M.S. performed the bioinformatic analyses. J.Y.F. and
558 G.C. wrote the manuscript with input from all authors.
559

560 **Data Availability**

561 Proteomic data are available via ProteomeXchange with identifier PXD017480.
562 Gene Ontology analysis pipeline is available via Github:
563 (https://github.com/DanielleMStevens/Franco_2020_Proteomics_Paper)
564

565 **Competing Financial Interests**

566 The authors declare no competing financial interest.

567 **References**

568 1. Li, J., Li, L., Pang, Z., Kolbasov, V. G., Ehsani, R., Carter, E. W., and Wang, N. (2019)
569 Developing citrus huanglongbing (HLB) management strategies based on the severity of
570 symptoms in HLB-endemic citrus-producing regions. *Phytopathology*. **109**, 582–592

571 2. Deng, H., Achor, D., Exteberria, E., Yu, Q., Du, D., Stanton, D., Liang, G., and Gmitter,
572 F. G. (2019) Phloem regeneration is a mechanism for huanglongbing-tolerance of "bearss"
573 lemon and "LB8-9" sugar belleopenspisupspi®closespisupspi mandarin. *Front. Plant Sci.*
574 **10**, 277

575 3. Ramadugu, C., Keremane, M. L., Halbert, S. E., Duan, Y. P., Roose, M. L., Stover, E.,
576 and Lee, R. F. (2016) Long-term field evaluation reveals Huanglongbing resistance in
577 Citrus relatives. *Plant Dis.* **100**, 1858–1869

578 4. da Graça, J. V., Douhan, G. W., Halbert, S. E., Keremane, M. L., Lee, R. F., Vidalakis, G.,
579 and Zhao, H. (2016) Huanglongbing: An overview of a complex pathosystem ravaging the
580 world's citrus. *J. Integr. Plant Biol.* **58**, 373–387

581 5. Dai, Z., Wu, F., Zheng, Z., Yokomi, R., Kumagai, L., Cai, W., Rascoe, J., Polek, M.,
582 Chen, J., and Deng, X. (2019) Prophage diversity of 'candidatus liberibacter asiaticus'
583 strains in California. *Phytopathology*. **109**, 551–559

584 6. McRoberts, N., Figuera, S. G., Olkowski, S., McGuire, B., Luo, W., Posny, D., and
585 Gottwald, T. (2019) Using models to provide rapid programme support for California's
586 efforts to suppress Huanglongbing disease of citrus. *Philos. Trans. R. Soc. B Biol. Sci.*
587 **374**, 1–11

588 7. Hodges, A. W., and Spreen, T. H. (2015) Economic Impacts of Citrus Greening -(HLB) in
589 Florida, 2006/07-2010/11. Univ Florida IFAS Ext., 7–12.

590 8. United States Department of Agriculture (USDA), N. A. S. S. (2017) Citrus Maturity Test
591 Results and Fruit Size.

592 9. Hung, T. H., Hung, S. C., Chen, C. N., Hsu, M. H., and Su, H. J. (2004) Detection by PCR
593 of Candidatus Liberibacter asiaticus, the bacterium causing citrus huanglongbing in vector
594 psyllids: Application to the study of vector-pathogen relationships. *Plant Pathol.* **53**, 96–
595 102

596 10. Hijaz, F., and Killiny, N. (2014) Collection and chemical composition of phloem sap from
597 Citrus sinensis L. Osbeck (sweet orange). *PLoS One*. **9**, e101830

598 11. Skryhan, K., Gurrieri, L., Sparla, F., Trost, P., and Blennow, A. (2018) Redox regulation
599 of starch metabolism. *Front. Plant Sci.* **9**, 1–8

600 12. Koh, E. J., Zhou, L., Williams, D. S., Park, J., Ding, N., Duan, Y. P., and Kang, B. H.
601 (2012) Callose deposition in the phloem plasmodesmata and inhibition of phloem
602 transport in citrus leaves infected with "Candidatus Liberibacter asiaticus." *Protoplasma*.
603 **249**, 687–697

604 13. Hu, Y., Zhong, X., Liu, X., Lou, B., Zhou, C., and Wang, X. (2017) Comparative
605 transcriptome analysis unveils the tolerance mechanisms of Citrus hystrix in response to

606 "Candidatus Liberibacter Asiaticus" infection. *PLoS One*. **12**, e0189229

607 14. Wang, N., and Trivedi, P. (2013) Citrus Huanglongbing: A Newly Relevant Disease
608 Presents Unprecedented Challenges. *Phytopathology*. **103**, 652–665

609 15. Bové, J. M. (2006) Huanglongbing: A destructive, newly-emerging, century-old disease of
610 citrus. *J. Plant Pathol.* **88**, 7–37

611 16. Dodds, P. N., and Rathjen, J. P. (2010) Plant immunity: towards an integrated view of
612 plant–pathogen interactions. *Nat. Rev. Genet.* **11**, 539–548

613 17. Cong, Q., Kinch, L. N., Kim, B. H., and Grishin, N. V. (2012) Predictive sequence
614 analysis of the Candidatus liberibacter asiaticus proteome. *PLoS One*. **7**, e41071

615 18. Yan, Q., Sreedharan, A., Wei, S., Wang, J., Pelz-Stelinski, K., Folimonova, S., and Wang,
616 N. (2013) Global gene expression changes in Candidatus Liberibacter asiaticus during the
617 transmission in distinct hosts between plant and insect. *Mol. Plant Pathol.* **14**, 391–404

618 19. Sugio, A., Kingdom, H. N., MacLean, A. M., Grieve, V. M., and Hogenhout, S. A. (2011)
619 Phytoplasma protein effector SAP11 enhances insect vector reproduction by manipulating
620 plant development and defense hormone biosynthesis. *Proc. Natl. Acad. Sci.* **108**, E1254–
621 E1263

622 20. Prasad, S., Xu, J., Zhang, Y., and Wang, N. (2016) SEC-translocon dependent
623 extracytoplasmic proteins of Candidatus liberibacter asiaticus. *Front. Microbiol.* **7**, 1–9

624 21. Thapa, S.P.;De Francesco, A; Trinh, J; Gurung, F.B.; Pang, Z; Vidalakis, G; Wang, N;
625 Ancona, V; Ma, W; Coaker, G. (2020) Genome-wide analyses of Liberibacter species
626 provides insights into evolution, phylogenetic relationships and virulence factors. *Mol.*
627 *Plant Pathol.* **00**, 1–16

628 22. Pitino, M., Armstrong, C. M., Cano, L. M., and Duan, Y. (2016) Transient expression of
629 Candidatus Liberibacter asiaticus effector induces cell death in Nicotiana benthamiana.
630 *Front Plant Sci*. **7**, 982

631 23. Clark, K., Franco, J. Y., Schwizer, S., Pang, Z., Hawara, E., Liebrand, T. W. H.,
632 Pagliaccia, D., Zeng, L., Gurung, F. B., Wang, P., Shi, J., Wang, Y., Ancona, V., Van Der
633 Hoorn, R. A. L., Wang, N., Coaker, G., and Ma, W. (2018) An effector from the
634 Huanglongbing-associated pathogen targets citrus proteases. *Nat. Commun.* **9**, 1718

635 24. Jain, M., Munoz-Bodnar, A., Zhang, S., and Gabriel, D. W. (2018) A secreted 'candidatus
636 liberibacter asiaticus' peroxiredoxin simultaneously suppresses both localized and
637 systemic innate immune responses in planta. *Mol. Plant-Microbe Interact.* **12**, 1312–1322

638 25. Wang, N., Pierson, E. A., Setubal, C., Xu, J., Levy, J. G., Zhang, Y., Li, J., Rangel, L. T.,
639 and Jr, J. M. (2017) Liberibacter – Host Interface : Insights into Pathogenesis Mechanisms
640 and Disease Control. *Annu. Rev. Phytopathol.* **55**, 1–32

641 26. Li, J., Pang, Z., Trivedi, P., Zhou, X., Ying, X., Jia, H., and Wang, N. (2017) "Candidatus
642 Liberibacter asiaticus" encodes a functional salicylic acid (SA) hydroxylase that degrades
643 SA to suppress plant defenses. *Mol. Plant-Microbe Interact.* **30**, 620–630

644 27. Zhang, J., and Zhou, J. M. (2010) Plant immunity triggered by microbial molecular
645 signatures. *Mol. Plant*. **3**, 783–793

646 28. Dalio, R. J. D., Magalhaes, D. M., Rodrigues, C. M., Arena, G. D., Oliveira, T. S., Souza-
647 Neto, R. R., Picchi, S. C., Martins, P. M. M., Santos, P. J. C., Maximo, H. J., Pacheco, I.
648 S., De Souza, A. A., and Machado, M. A. (2017) PAMPs, PRRs, effectors and R-genes
649 associated with citrus-pathogen interactions. *Ann. Bot.* **120**, 617

650 29. Jain, M., Fleites, L. A., and Gabriel, D. W. (2015) Prophage-encoded peroxidase in
651 "candidatus liberibacter asiaticus" is a secreted effector that suppresses plant defenses.
652 *Mol. Plant-Microbe Interact.* **28**, 1330–7

653 30. Liao, H. L., and Burns, J. K. (2012) Gene expression in Citrus sinensis fruit tissues
654 harvested from huanglongbing-infected trees: Comparison with girdled fruit. *J. Exp. Bot.*
655 **63**, 3307–19

656 31. Fan, J., Chen, C., Yu, Q., Brlansky, R. H., Li, Z. G., and Gmitter, F. G. (2011)
657 Comparative iTRAQ proteome and transcriptome analyses of sweet orange infected by
658 "Candidatus Liberibacter asiaticus." *Physiol. Plant.* **143**, 235–245

659 32. Albrecht, U., and Bowman, K. D. (2012) Transcriptional response of susceptible and
660 tolerant citrus to infection with Candidatus Liberibacter asiaticus. *Plant Sci.* **185–186**,
661 118–130

662 33. Albrecht, U., and Bowman, K. D. (2008) Gene expression in Citrus sinensis (L.) Osbeck
663 following infection with the bacterial pathogen Candidatus Liberibacter asiaticus causing
664 Huanglongbing in Florida. *Plant Sci.* **175**, 291–306

665 34. Kim, J.-S., Sagaram, U. S., Burns, J. K., Li, J.-L., and Wang, N. (2009) Response of sweet
666 orange (Citrus sinensis) to "Candidatus Liberibacter asiaticus" infection: microscopy and
667 microarray analyses. *Phytopathology*. **99**, 50–57

668 35. Zhong, Y., Cheng, C. Z., Jiang, N. H., Jiang, B., Zhang, Y. Y., Wu, B., Hu, M. L., Zeng, J.
669 W., Yan, H. X., Yi, G. J., and Zhong, G. Y. (2015) Comparative transcriptome and
670 iTRAQ proteome analyses of citrus root responses to candidatus liberibacter asiaticus
671 infection. *PLoS One*. **10**, e0126973

672 36. Aritua, V., Achor, D., Gmitter, F. G., Albrigo, G., and Wang, N. (2013) Transcriptional
673 and Microscopic Analyses of Citrus Stem and Root Responses to Candidatus Liberibacter
674 asiaticus Infection. *PLoS One*. **8**, e73742

675 37. Etxeberria, E., Gonzalez, P., Achor, D., and Albrigo, G. (2009) Anatomical distribution of
676 abnormally high levels of starch in HLB-affected Valencia orange trees. *Physiol. Mol.*
677 *Plant Pathol.* **74**, 76–83

678 38. Li, W., Hartung, J. S., and Levy, L. (2006) Quantitative real-time PCR for detection and
679 identification of Candidatus Liberibacter species associated with citrus huanglongbing. *J.*
680 *Microbiol. Methods*. **66**, 104–15

681 39. Trivedi, P., Sagaram, U. S., Kim, J. S., Brlansky, R. H., Rogers, M. E., Stelinski, L. L.,
682 Oswalt, C., and Wang, N. (2009) Quantification of viable Candidatus Liberibacter
683 asiaticus in hosts using quantitative PCR with the aid of ethidium monoazide (EMA). *Eur.*

684 *J. Plant Pathol.* **124**, 553–563

685 40. Shevchenko, A., Tomas, H., Havliš, J., Olsen, J. V., and Mann, M. (2006) In-gel digestion
686 for mass spectrometric characterization of proteins and proteomes. *Nat. Protoc.* **1**, 2856–
687 60

688 41. Cox, J., and Mann, M. (2008) MaxQuant enables high peptide identification rates,
689 individualized p.p.b.-range mass accuracies and proteome-wide protein quantification.
690 *Nat. Biotechnol.* **26**, 1367–1372

691 42. Cox, J., Neuhauser, N., Michalski, A., Scheltema, R. A., Olsen, J. V., and Mann, M.
692 (2011) Andromeda: A peptide search engine integrated into the MaxQuant environment.
693 *J. Proteome Res.* **10**, 1794–1805

694 43. Goodstein, D. M., Shu, S., Howson, R., Neupane, R., Hayes, R. D., Fazo, J., Mitros, T.,
695 Dirks, W., Hellsten, U., Putnam, N., and Rokhsar, D. S. (2012) Phytozome: A
696 comparative platform for green plant genomics. *Nucleic Acids Res.* **40**, D1178-86

697 44. Duan, Y., Zhou, L., Hall, D. G., Li, W., Doddapaneni, H., Lin, H., Liu, L., Vahling, C. M.,
698 Gabriel, D. W., Williams, K. P., Dickerman, A., Sun, Y., and Gottwald, T. (2009)
699 Complete genome sequence of citrus huanglongbing bacterium, "Candidatus Liberibacter
700 asiaticus" obtained through metagenomics. *Mol. Plant. Microbe. Interact.* **22**, 1011–1020

701 45. Tyanova, S., Temu, T., Sinitcyn, P., Carlson, A., Hein, M. Y., Geiger, T., Mann, M., and
702 Cox, J. (2016) The Perseus computational platform for comprehensive analysis of
703 (prote)omics data. *Nat. Methods*. **13**, 731–740

704 46. Perez-Riverol, Y., Csordas, A., Bai, J., Bernal-Llinares, M., Hewapathirana, S., Kundu, D.
705 J., Inuganti, A., Griss, J., Mayer, G., Eisenacher, M., Pérez, E., Uszkoreit, J., Pfeuffer, J.,
706 Sachsenberg, T., Yilmaz, Ş., Tiwary, S., Cox, J., Audain, E., Walzer, M., Jarnuczak, A. F.,
707 Ternent, T., Brazma, A., and Vizcaíno, J. A. (2019) The PRIDE database and related tools
708 and resources in 2019: Improving support for quantification data. *Nucleic Acids Res.* **47**,
709 D442–D450

710 47. Gu, Z., Eils, R., and Schlesner, M. (2016) Complex heatmaps reveal patterns and
711 correlations in multidimensional genomic data. *Bioinformatics*. **32**, 2847–9

712 48. Carella, P., Wilson, D. C., Kempthorne, C. J., and Cameron, R. K. (2016) Vascular sap
713 proteomics: Providing insight into long-distance signaling during stress. *Front. Plant Sci.*
714 **7**, 1–8

715 49. Carella, P., Merl-Pham, J., Wilson, D. C., Dey, S., Hauck, S. M., Vlot, A. C., and
716 Cameron, R. K. (2016) Comparative proteomics analysis of phloem exudates collected
717 during the induction of systemic acquired resistance. *Plant Physiol.* **171**, 1495–510

718 50. Huang, S., Li, R., Zhang, Z., Li, L., Gu, X., Fan, W., Lucas, W. J., Wang, X., Xie, B., Ni,
719 P., Ren, Y., Zhu, H., Li, J., Lin, K., Jin, W., Fei, Z., Li, G., Staub, J., Kilian, A., Van Der
720 Vossen, E. A. G., Wu, Y., Guo, J., He, J., Jia, Z., Ren, Y., Tian, G., Lu, Y., Ruan, J., Qian,
721 W., Wang, M., Huang, Q., Li, B., Xuan, Z., Cao, J., Asan, Wu, Z., Zhang, J., Cai, Q., Bai,
722 Y., Zhao, B., Han, Y., Li, Y., Li, X., Wang, S., Shi, Q., Liu, S., Cho, W. K., Kim, J. Y.,
723 Xu, Y., Heller-Uszynska, K., Miao, H., Cheng, Z., Zhang, S., Wu, J., Yang, Y., Kang, H.,

724 Li, M., Liang, H., Ren, X., Shi, Z., Wen, M., Jian, M., Yang, H., Zhang, G., Yang, Z.,
725 Chen, R., Liu, S., Li, J., Ma, L., Liu, H., Zhou, Y., Zhao, J., Fang, X., Li, G., Fang, L., Li,
726 Y., Liu, D., Zheng, H., Zhang, Y., Qin, N., Li, Z., Yang, G., Yang, S., Bolund, L.,
727 Kristiansen, K., Zheng, H., Li, S., Zhang, X., Yang, H., Wang, J., Sun, R., Zhang, B.,
728 Jiang, S., Wang, J., Du, Y., and Li, S. (2009) The genome of the cucumber, Cucumis
729 sativus L. *Nat. Genet.* **41**, 1275–81

730 51. Wilkinson, L. (2012) Exact and approximate area-proportional circular venn and euler
731 diagrams. *IEEE Trans. Vis. Comput. Graph.* **18**, 321–31

732 52. Gu, Z., Gu, L., Eils, R., Schlesner, M., and Brors, B. (2014) Circlize implements and
733 enhances circular visualization in R. *Bioinformatics*. **30**, 2811–2

734 53. Wu, G. A., Prochnik, S., Jenkins, J., Salse, J., Hellsten, U., Murat, F., Perrier, X., Ruiz,
735 M., Scalabrin, S., Terol, J., Takita, M. A., Labadie, K., Poulain, J., Couloux, A., Jabbari,
736 K., Cattonaro, F., Del Fabbro, C., Pinosio, S., Zuccolo, A., Chapman, J., Grimwood, J.,
737 Tadeo, F. R., Estornell, L. H., Muñoz-Sanz, J. V., Ibanez, V., Herrero-Ortega, A., Aleza,
738 P., Pérez-Pérez, J., Ramón, D., Brunel, D., Luro, F., Chen, C., Farmerie, W. G., Desany,
739 B., Kodira, C., Mohiuddin, M., Harkins, T., Fredrikson, K., Burns, P., Lomsadze, A.,
740 Borodovsky, M., Reforgiato, G., Freitas-Astúa, J., Quetier, F., Navarro, L., Roose, M.,
741 Wincker, P., Schmutz, J., Morgante, M., MacHado, M. A., Talon, M., Jaillon, O.,
742 Ollitrault, P., Gmitter, F., and Rokhsar, D. (2014) Sequencing of diverse mandarin,
743 pummelo and orange genomes reveals complex history of admixture during citrus
744 domestication. *Nat. Biotechnol.* **32**, 656–62

745 54. Löytynoja, A. (2014) Phylogeny-aware alignment with PRANK. *Methods Mol. Biol.*
746 **1079**, 155–70

747 55. Stamatakis, A. (2006) RAxML-VI-HPC: Maximum likelihood-based phylogenetic
748 analyses with thousands of taxa and mixed models. *Bioinformatics*. **22**, 2688–90

749 56. Rambaut, A. (2016) FigTree v1.4.3. *Mol. Evol. phylogenetics Epidemiol.* Available at:
750 http://tree.bio.ed.ac.uk/software/figtree/.

751 57. Adam Mott, G., Desveaux, D., and Guttman, D. S. (2018) A high-sensitivity, microtiter-
752 based plate assay for plant pattern-triggered immunity. *Mol. Plant-Microbe Interact.* **31**,
753 499–504

754 58. Xu, Q., Chen, L. L., Ruan, X., Chen, D., Zhu, A., Chen, C., Bertrand, D., Jiao, W. B.,
755 Hao, B. H., Lyon, M. P., Chen, J., Gao, S., Xing, F., Lan, H., Chang, J. W., Ge, X., Lei,
756 Y., Hu, Q., Miao, Y., Wang, L., Xiao, S., Biswas, M. K., Zeng, W., Guo, F., Cao, H.,
757 Yang, X., Xu, X. W., Cheng, Y. J., Xu, J., Liu, J. H., Luo, O. J., Tang, Z., Guo, W. W.,
758 Kuang, H., Zhang, H. Y., Roose, M. L., Nagarajan, N., Deng, X. X., and Ruan, Y. (2013)
759 The draft genome of sweet orange (Citrus sinensis). *Nat. Genet.* **45**, 59–66

760 59. Kennedy, J. S., and Mittler, T. E. (1953) A Method of obtaining Phloem Sap via the
761 Mouth-parts of Aphids. *Nature*. **171**, 528

762 60. Dinant, S., Bonnemain, J. L., Girousse, C., and Kehr, J. (2010) Phloem sap intricacy and
763 interplay with aphid feeding. *Comptes Rendus - Biol.* **333**, 504–15

764 61. Zipfel, C. (2014) Plant pattern-recognition receptors. *Trends Immunol.* **35**, 345–51

765 62. Misas-Villamil, J. C., van der Hoorn, R. A. L., and Doehlemann, G. (2016) Papain-like
766 cysteine proteases as hubs in plant immunity. *New Phytol.* **212**, 902–907

767 63. Jashni, M. K., Mehrabi, R., Collemare, J., Mesarich, C. H., and de Wit, P. J. G. M. (2015)
768 The battle in the apoplast: further insights into the roles of proteases and their inhibitors in
769 plant–pathogen interactions. *Front. Plant Sci.* **6**, 1–7

770 64. Passardi, F., Cosio, C., Penel, C., and Dunand, C. (2005) Peroxidases have more functions
771 than a Swiss army knife. *Plant Cell Rep.* **24**, 255–65

772 65. Almagro, L., Gómez Ros, L. V., Belchi-Navarro, S., Bru, R., Ros Barceló, A., and
773 Pedreño, M. A. (2009) Class III peroxidases in plant defence reactions. *J. Exp. Bot.* **60**,
774 377–90

775 66. Pandey, V. P., Awasthi, M., Singh, S., Tiwari, S., and Dwivedi, U. N. (2017) A
776 Comprehensive Review on Function and Application of Plant Peroxidases. *Biochem.*
777 *Anal. Biochem.* **6**, 1–16

778 67. Passardi, F., Theiler, G., Zamocky, M., Cosio, C., Rouhier, N., Teixera, F., Margis-
779 Pinheiro, M., Ioannidis, V., Penel, C., Falquet, L., and Dunand, C. (2007) PeroxiBase: The
780 peroxidase database. *Phytochemistry*. **68**, 1605–11

781 68. Hiraga, S., Sasaki, K., Ito, H., Ohashi, Y., and Matsui, H. (2001) A large family of class
782 III plant peroxidases. *Plant Cell Physiol.* **42**, 462–8

783 69. Cosio, C., and Dunand, C. (2009) Specific functions of individual class III peroxidase
784 genes. *J. Exp. Bot.* **60**, 391–408

785 70. Putnam, A. H., and Hudson, M. E. (2018) Florida Citrus Statistics 2016-2017. *Florida*
786 *Department of Agriulture and Consumer Services.* Available at:
787 https://www.nass.usda.gov/

788 71. Miller, C. S. I. D. (2017) Texas Citrus Nursery Stock Certification Manual TEXAS
789 DEPARTMENT OF AGRICULTURE. Agriculture and Consumer Protection Division,
790 Environmental and Biosecurity Programs, Citrus Program. Available at:
791 https://www.texasagriculture.gov/

792 72. Rawlings, N. D., Barrett, A. J., Thomas, P. D., Huang, X., Bateman, A., and Finn, R. D.
793 (2018) The MEROPS database of proteolytic enzymes, their substrates and inhibitors in
794 2017 and a comparison with peptidases in the PANTHER database. *Nucleic Acids Res.* **46**,
795 D624–D632

796 73. van der Hoorn, R. A. L. (2008) Plant Proteases: From Phenotypes to Molecular
797 Mechanisms. *Annu. Rev. Plant Biol.* **59**, 191–223

798 74. Sueldo, D., Ahmed, A., Misas-Villamil, J., Colby, T., Tameling, W., Joosten, M. H. A. J.,
799 and Van der Hoorn, R. A. L. (2014) Dynamic hydrolase activities precede hypersensitive
800 tissue collapse in tomato seedlings. *New Phytol.* **203**, 913–925

801 75. Di Cera, E. (2009) Serine proteases. *IUBMB Life*. 10.1002/iub.186

802 76. Figueiredo, J., Sousa Silva, M., and Figueiredo, A. (2018) Subtilisin-like proteases in
803 plant defence: the past, the present and beyond. *Mol. Plant Pathol.* **19**, 1017–1028

804 77. Thomas, E. L., and van der Hoorn, R. A. L. (2018) Ten prominent host proteases in plant-
805 pathogen interactions. *Int. J. Mol. Sci.* **19**, E639

806 78. Rustgi, S., Boex-Fontvieille, E., Reinbothe, C., von Wettstein, D., and Reinbothe, S.
807 (2018) The complex world of plant protease inhibitors: Insights into a Kunitz-type
808 cysteine protease inhibitor of Arabidopsis thaliana. *Commun. Integr. Biol.* **11**, e1368599

809 79. Martinez, M., Cambra, I., Carrillo, L., Diaz-Mendoza, M., and Diaz, I. (2009)
810 Characterization of the entire cystatin gene family in barley and their target cathepsin L-
811 like cysteine-proteases, partners in the hordein mobilization during seed germination.
812 *Plant Physiol.* **151**, 1531–45

813 80. Cohen, M., Davydov, O., and Fluhr, R. (2019) Plant serpin protease inhibitors: Specificity
814 and duality of function. *J. Exp. Bot.* **70**, 2077–2085

815 81. van der Hoorn, R. A. L. (2004) Activity Profiling of Papain-Like Cysteine Proteases in
816 Plants. *PLANT Physiol.* **135**, 1170–8

817 82. Liu, Y., Patricelli, M. P., and Cravatt, B. F. (1999) Activity-based protein profiling: The
818 serine hydrolases. *Proc. Natl. Acad. Sci. U. S. A.* **96**, 14694–9

819 83. Chin, E. L., Ramsey, J. S., Mishchuk, D. O., Saha, S., Foster, E., Chavez, J. D., Howe, K.,
820 Zhong, X., Polek, M., Godfrey, K. E., Mueller, L., Bruce, J. E., Heck, M., and Slupsky, C.
821 M. (2019) Longitudinal transcriptomic, proteomic, and metabolomic analyses of Citrus
822 sinensis (L.) Osbeck graft-inoculated with 'Candidatus Liberibacter asiaticus.' *J.*
823 *Proteome Res.* **19**, 719–732

824 84. Wang, Y., Zhou, L., Yu, X., Stover, E., Luo, F., and Duan, Y. (2016) Transcriptome
825 profiling of huanglongbing (HLB) tolerant and susceptible citrus plants reveals the role of
826 basal resistance in HLB tolerance. *Front. Plant Sci.* **7**, 1–13

827 85. Yu, Q., Chen, C., Du, D., Huang, M., Yao, J., Yu, F., Brlansky, R. H., and Gmitter, F. G.
828 (2017) Reprogramming of a defense signaling pathway in rough lemon and sweet orange
829 is a critical element of the early response to Candidatus Liberibacter asiaticus. *Hortic. Res.*
830 **4**, 1–15

831 86. Nwugo, C. C., Lin, H., Duan, Y., and Civerolo, E. L. (2013) The effect of "Candidatus
832 Liberibacter asiaticus" infection on the proteomic profiles and nutritional status of pre-
833 symptomatic and symptomatic grapefruit (Citrus paradisi) plants. *BMC Plant Biol.* **13**, 1–
834 24

835 87. Khairulmazmi Ahmad (2011) Field assessment of calcium, copper and zinc ions on plant
836 recovery and disease severity following infection of Huanglongbing (HLB) disease.
837 *African J. Microbiol. Res.* **5**, 4967–4979

838 88. Huot, B., Yao, J., Montgomery, B. L., and He, S. Y. (2014) Growth-defense tradeoffs in
839 plants: A balancing act to optimize fitness. *Mol. Plant*. **7**, 1267–1287

840 89. Apel, K., and Hirt, H. (2004) REACTIVE OXYGEN SPECIES: Metabolism, Oxidative

841 Stress, and Signal Transduction. *Annu. Rev. Plant Biol.* **55**, 373–99

842 90. Serra-Soriano, M., Navarro, J. A., Genoves, A., and Pallás, V. (2015) Comparative
843 proteomic analysis of melon phloem exudates in response to viral infection. *J. Proteomics*.
844 **124**, 11–24

845 91. Martinelli, F., Reagan, R. L., Dolan, D., Fileccia, V., and Dandekar, A. M. (2016)
846 Proteomic analysis highlights the role of detoxification pathways in increased tolerance to
847 Huanglongbing disease. *BMC Plant Biol.* **16**, 167

848 92. Nwugo, C. C., Doud, M. S., Duan, Y. ping, and Lin, H. (2016) Proteomics analysis
849 reveals novel host molecular mechanisms associated with thermotherapy of 'Ca.
850 Liberibacter asiaticus'-infected citrus plants. *BMC Plant Biol.* **16**, 253

851 93. Balan, B., Ibáñez, A. M., Dandekar, A. M., Caruso, T., and Martinelli, F. (2018)
852 Identifying host molecular features strongly linked with responses to huanglongbing
853 disease in citrus leaves. *Front. Plant Sci.* **9**, 1–13

854 94. Kehr, J. (2006) Phloem sap proteins: Their identities and potential roles in the interaction
855 between plants and phloem-feeding insects. *J. Exp. Bot.* **57**, 767–74

856 95. Walz, C., Giavalisco, P., Schad, M., Juenger, M., Klose, J., and Kehr, J. (2004)
857 Proteomics of curcurbit phloem exudate reveals a network of defence proteins.
858 *Phytochemistry*. **65**, 1795–804

859 96. Petzold, H. E., Zhao, M., and Beers, E. P. (2012) Expression and functions of proteases in
860 vascular tissues. *Physiol. Plant.* **145**, 121–9

861 97. Hu, C., Ham, B. K., El-shabrawi, H. M., Alexander, D., Zhang, D., Ryals, J., and Lucas,
862 W. J. (2016) Proteomics and metabolomics analyses reveal the cucurbit sieve tube system
863 as a complex metabolic space. *Plant J.* **87**, 442–454

864 98. Hao, G., Pitino, M., Duan, Y., and Stover, E. (2016) Reduced Susceptibility to
865 Xanthomonas citri in Transgenic Citrus Expressing the FLS2 Receptor From Nicotiana
866 benthamiana. *Mol. Plant-Microbe Interact.* **29**, 132–42

867 99. Ilyas, M., Hörger, A. C., Bozkurt, T. O., Van Den Burg, H. A., Kaschani, F., Kaiser, M.,
868 Belhaj, K., Smoker, M., Joosten, M. H. A. J., Kamoun, S., and Van Der Hoorn, R. A. L.
869 (2015) Functional Divergence of Two Secreted Immune Proteases of Tomato. *Curr. Biol.*
870 **25**, 2300–2306

871 100. Lozano-Torres, J. L., Wilbers, R. H. P., Gawronski, P., Boshoven, J. C., Finkers-
872 Tomczak, A., Cordewener, J. H. G., America, A. H. P., Overmars, H. A., Van 't Klooster,
873 J. W., Baranowski, L., Sobczak, M., Ilyas, M., van der Hoorn, R. A. L., Schots, A., de
874 Wit, P. J. G. M., Bakker, J., Goverse, A., and Smant, G. (2012) Dual disease resistance
875 mediated by the immune receptor Cf-2 in tomato requires a common virulence target of a
876 fungus and a nematode. *Proc. Natl. Acad. Sci.* **109**, 10119–10124

877 101. Padhi, E. M. T., Maharaj, N., Lin, S. Y., Mishchuk, D. O., Chin, E., Godfrey, K., Foster,
878 E., Polek, M., Leveau, J. H. J., and Slupsky, C. M. (2019) Metabolome and microbiome
879 signatures in the roots of citrus affected by huanglongbing. *Phytopathology*. **109**, 2022–
880 2032

881 102. Wu, G. A., Terol, J., Ibanez, V., López-García, A., Pérez-Román, E., Borredá, C.,
882 Domingo, C., Tadeo, F. R., Carbonell-Caballero, J., Alonso, R., Curk, F., Du, D.,
883 Ollitrault, P., Roose, M. L., Dopazo, J., Gmitter, F. G., Rokhsar, D. S., and Talon, M.
884 (2018) Genomics of the origin and evolution of Citrus. *Nature*. **554**, 311–316

885
886

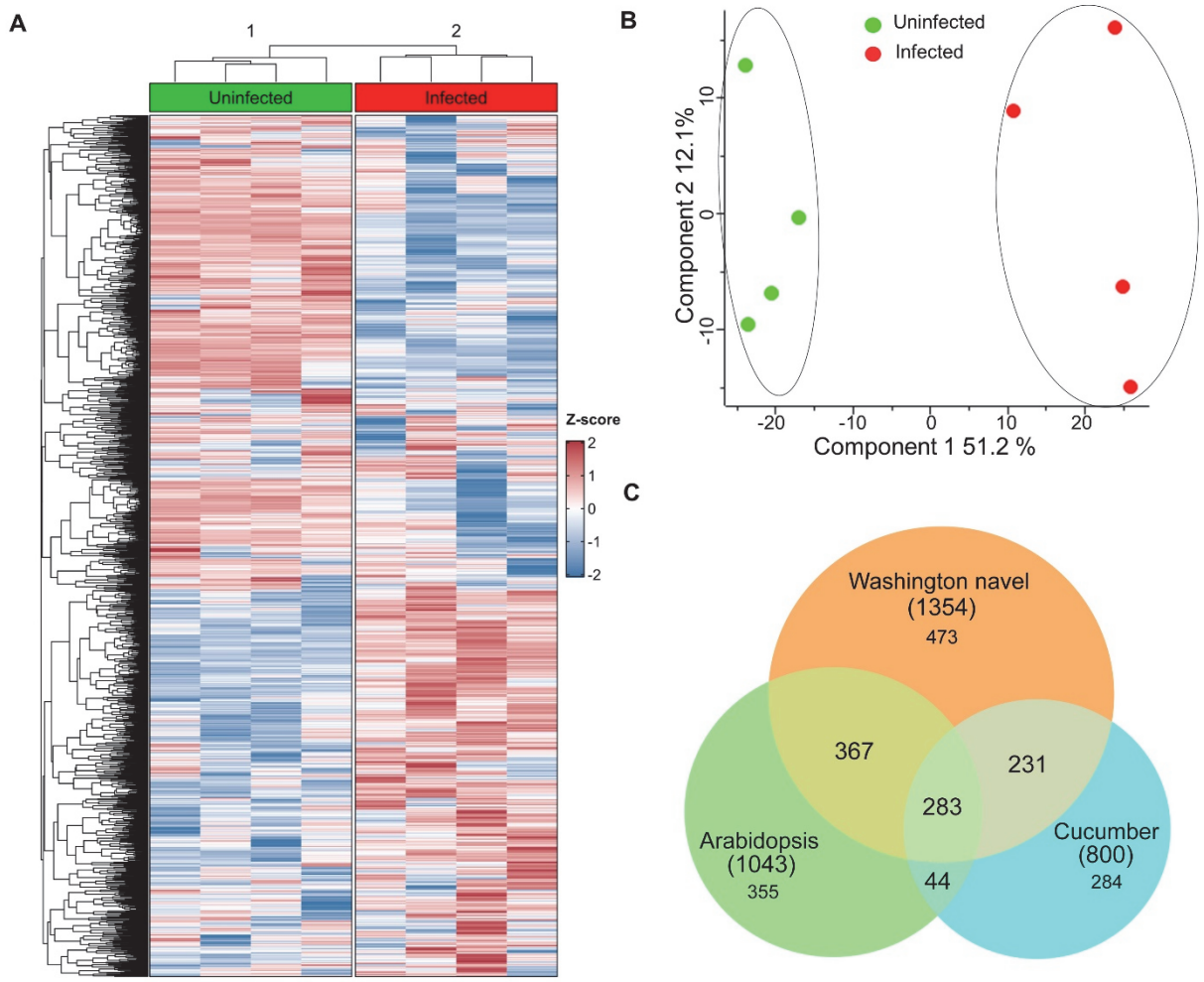

887

888 **Fig. 1. *C*Las induces global changes in protein expression in citrus vascular exudates (A)**
889 Heatmap of proteins identified in citrus sap exudates. Vascular proteins were enriched and
890 extracted from mock and *C*Las-graft inoculated Washington navel oranges (*C. sinensis* (L)
891 Osbeck) and subjected to label-free MS1 quantification. Identified proteins are shown in rows,
892 normalized by their mean value, and the Z-score was calculated for hierarchical clustering using
893 Euclidean distance. Columns represent biological replicates (individual trees). Red indicates
894 proteins where expression was increased, and blue indicates decreased protein expression
895 relative to the mean. **(B)** Principal component analyses (PCA) was performed on untransformed
896 label free quantification values in Perseus. **(C)** Comparison of phloem proteins identified in
897 diverse plant species. A total of 1354 proteins from Washington navel identified from this study
898 were compared with previous phloem proteomics studies in *Arabidopsis thaliana* and cucumber

899 (*Cucumis sativus*) phloem proteins using BLAST with an E-value of 1e-10 as a cutoff. The venn
900 diagram indicates protein overlap and was generated using the vennueler R package.

901

902

903

904

905

906

907

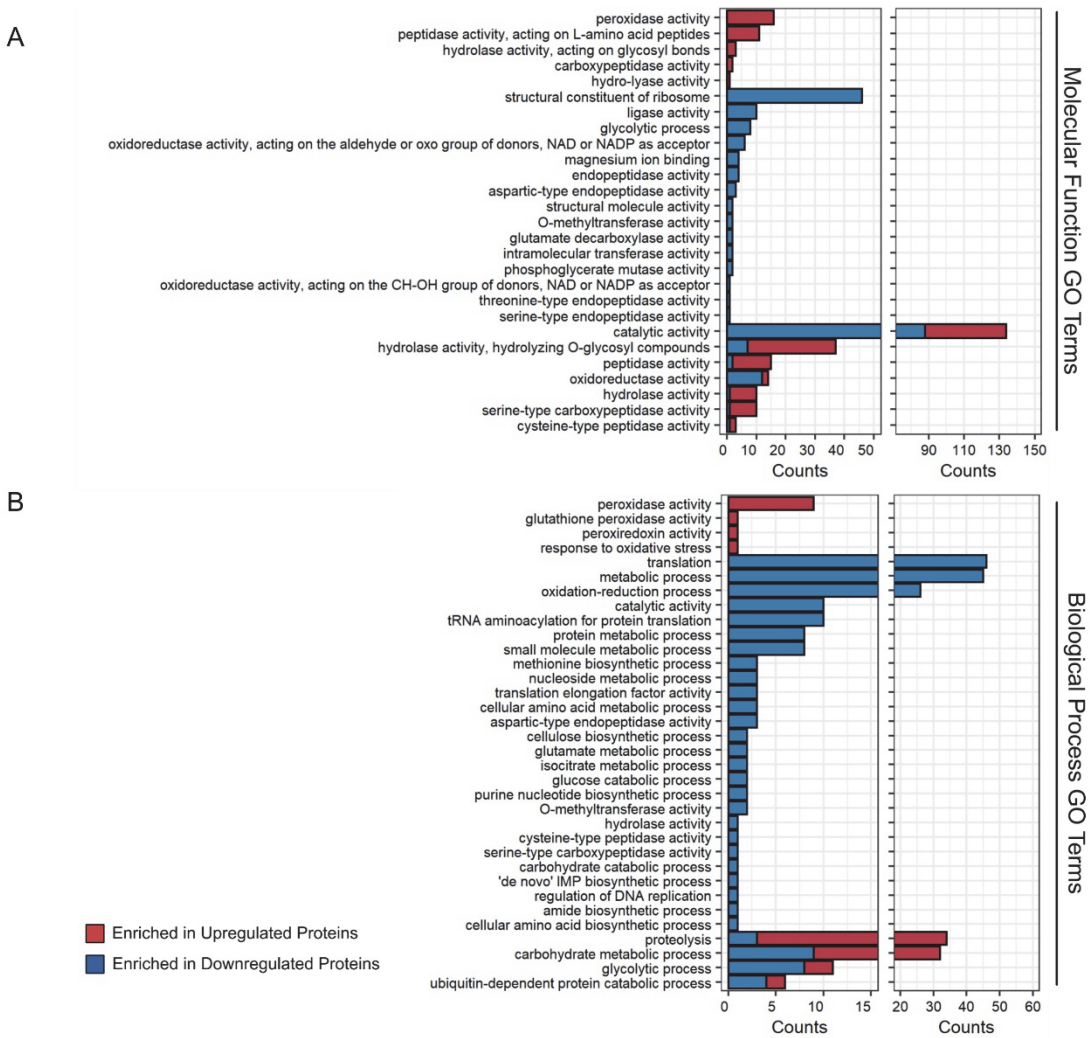

Fig. 2. Gene ontology (GO) analyses of citrus proteomics. (A) The biological processes and **(B)** molecular function of 692 significantly changing proteins identified by proteomics analyses of enriched vascular proteins from Washington navel ten months post-graft inoculation with *C*Las compared to mock inoculated controls. GO analyses and molecular function was performed using Phytozome 12 (https://phytozome.jgi.doe.gov/). Bonferroni was used for test correction with an FDR rate of <0.05. GO term slimming was performed manually by removing redundant terms used for the same group of proteins. Blue = enriched in downregulated proteins after graft inoculation with *C*Las; Red = enriched in upregulated proteins after graft inoculation with *C*Las.

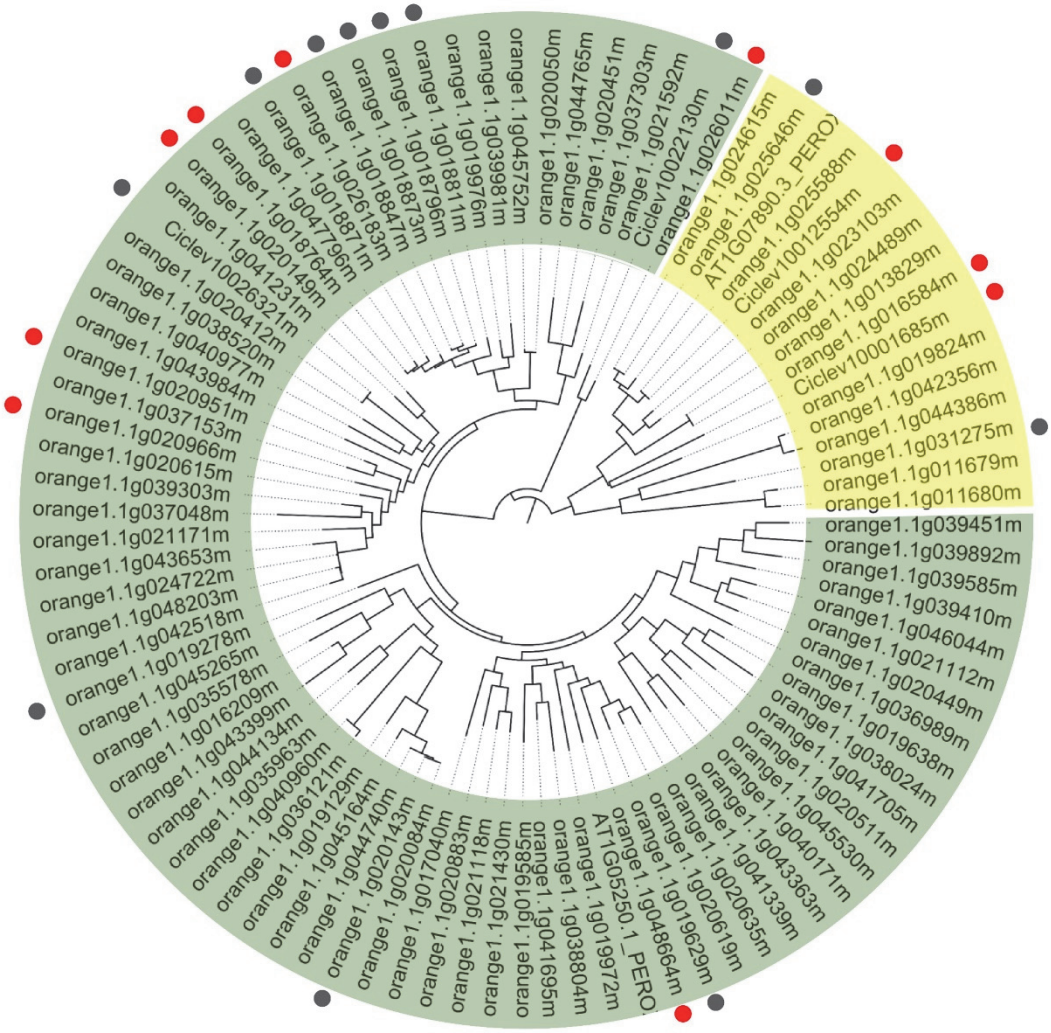

Fig. 3. Phylogenetic analyses reveal dynamic changes in specific citrus class I and III peroxidases after inoculation with *C*Las. A total of 15(13, *C. sinensis,* (*Cs*) and 2 *C. clementina,*(*Cc*)) Class I (yellow) and 78 (76 *Cs* , 2 Cc) Class III (green) peroxidases were identified from the citrus genome using the PF00141 Pfam domain and the RedOxiBase database. Two *Arabidopsis thaliana* sequences were used to guide clustering, one class I Peroxidase (AT1G07890.3) and one class III peroxidase (AT1G05250.1). Accession numbers starting with orange1.1g indicate proteins identified from the *C. sinensis* (navel) genome while those starting with Ciclev are those identified from the *C. clementina* (clementine) genome. Redundant sequences from *Citrus clementina* were removed from the phylogeny. A maximum likelihood approach was used to generate the phylogeny with 1000 bootstrap replicates. The resulting phylogeny was visualized using FigTree. A total of 22 peroxidases were

930 identified by mass spectrometry in Washington Navel. Red indicates peroxidases that were
931 significantly induced by mass spectrometry in *C*Las inoculated Washington navel and grey
932 indicates peroxidases that were detected, but not significantly changing after inoculation.

933

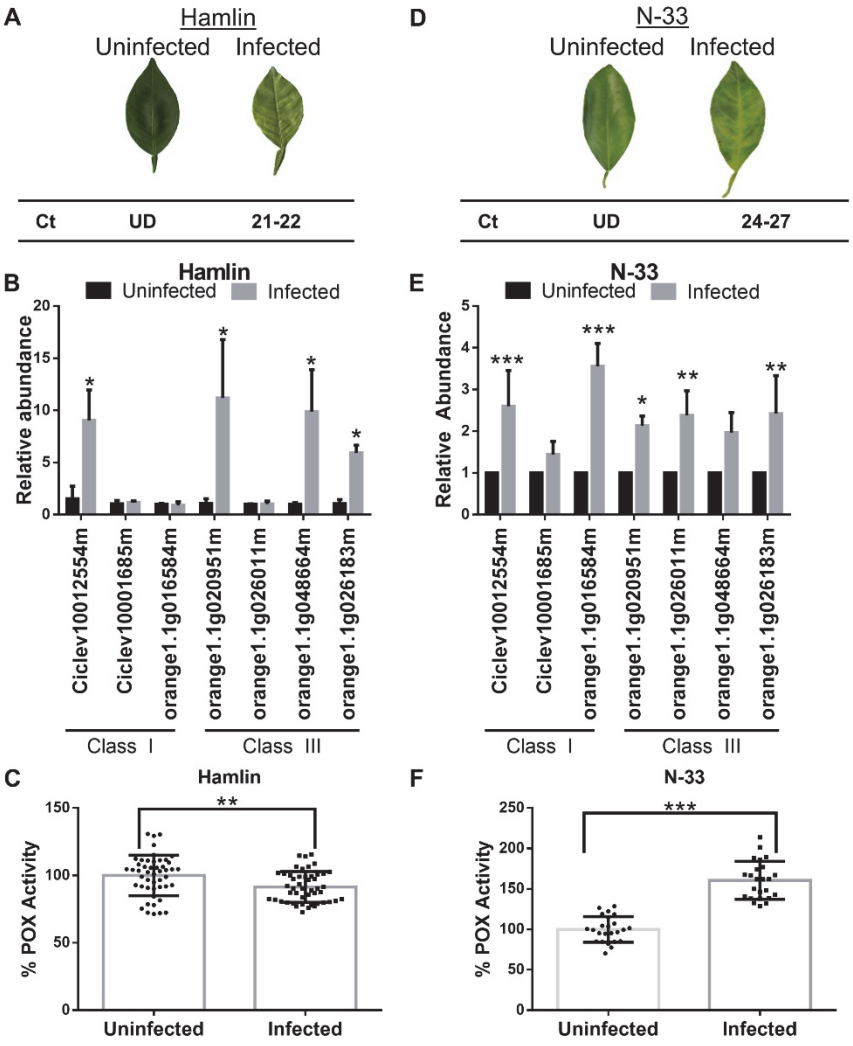

Fig 4. Peroxidase activity and transcript accumulation depend on citrus genotype. Two sweet orange varieties were inoculated with *C*Las using *Diaphorina citri* and analyzed for peroxidase (POX) enzymatic activity and transcript abundance. **(A)** HLB symptoms on representative Hamlin leaves (top) and corresponding Ct value for *C*Las (bottom) one year after feeding with *C*Las positive and negative *D. citri*. Citrus plants were grown under greenhouse conditions. *C*Las titers were detected by qPCR using primers targeting the β-operon (GenBank: AY342001.1). **(B)** Select peroxidase (POX) transcripts increase during infection in Hamlin. Hamlin trees were inoculated as described in (A) and RNA was extracted from the leaves. POXs that were significantly induced by proteomics analyses in Washington navel after CLas inoculation were analyzed for transcriptional expression using qPCR. Transcripts were normalized to GAPDH-C (NCBI Rseq: XM_006476919.3). Graphs show means ±SD, n= 4

946 trees. Significant differences were detected with a two-tailed unpaired Student's t-test, alpha-
947 value of 0.05. **(C)** POX enzymatic activity decreases during infection in Hamlin. Hamlin trees
948 were inoculated as described in (A) and POX activity was detected on leaf punches surrounding
949 the midrib one-year post-inoculation from the same leaves used for RNA extraction in (B).
950 Graphs show means ±SD, n=12 samples taken from 4 individual trees. Significant differences
951 were detected with a two-tailed unpaired Student's t-test, $p<0.01$. **(D)** HLB symptoms on
952 representative N-33 leaves (top) and corresponding Ct value for *C*Las (bottom). Citrus plants
953 were grown in a Texas field where *C*Las was naturally transmitted by *D. citri***.** Uninfected leaf
954 samples were taken from plants grown in an adjacent screenhouse. *C*Las titers were detected by
955 qPCR primers targeting the 16s rDNA (GenBank: L22532). **(E)** Select peroxidase transcripts
956 increase during infection in N-33. Leaf samples were taken from trees described in (D) and RNA
957 was extracted from leaf tissue. POXs that were significantly changing in Washington navel
958 proteomic analyses were selected and analyzed as described in (C). Graphs show mean ±SD,
959 n=3 trees. Significant differences were detected with a two-tailed unpaired Student's t-test,
960 Asterisks represent p values, *=<0.05, **=<0.01, ***=<0.001. Experiments were repeated three
961 times with similar results. **(F)** POX activity increases during infection in N-33. Leaf punches
962 from N-33 leaf samples taken from trees described in (D). Graphs show mean ±SD, n=8 taken
963 from 3 individual trees. Significant differences were detected with a two tailed unpaired
964 Student's t-test, $p<0.001$.

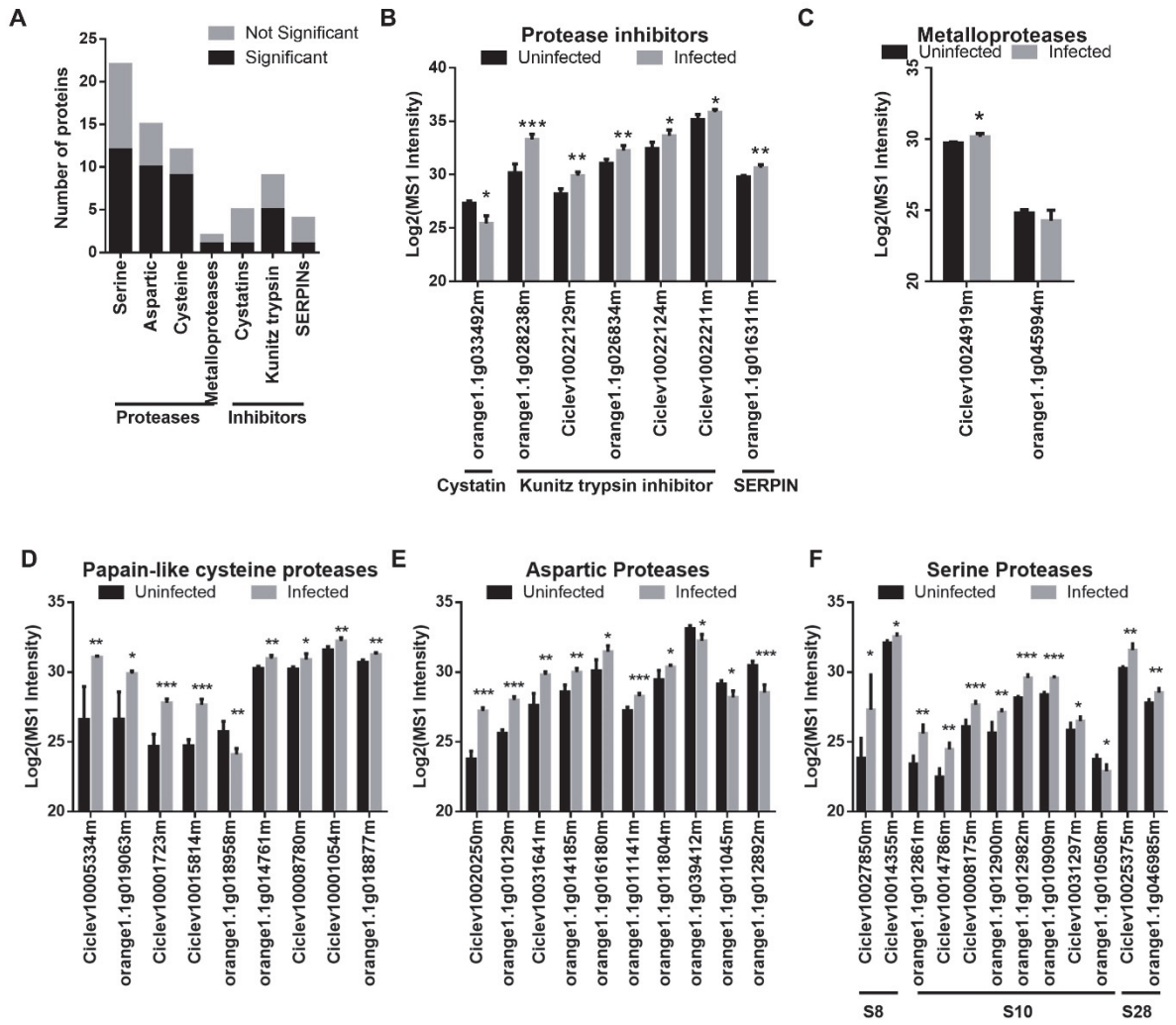

Fig 5. There is a dynamic interplay between the abundance of proteases and protease inhibitors during *C*Las infection. (A) Total number of proteases and protease inhibitors identified by proteomics analyses of enriched vascular proteins from Washington navel ten months post-graft inoculation with *C*Las compared to mock inoculated controls. Four proteases classes comprising: 22 serine proteases, 15 aspartic proteases, 12 cysteine proteases, and 2 metalloproteases were identified. Three protease inhibitor classes were identified: 5 cystatins, 12 serine protease inhibitors (9 Kunitz trypsin inhibitors and 4 SERPINs). Black indicates proteins that were significantly induced by mass spectrometry in *C*Las inoculated Washington navel and grey indicates proteins that were detected, but not significantly changing after inoculation. **(B-F)** Abundance of specific protease inhibitors and proteases that exhibit differential accumulation by mass spectrometry. Protein abundance is depicted as Log_2(MS1) intensity. Abundance in mock

977 inoculated is displayed in black and *C*Las inoculated in grey. Graphs indicate means ±SD, n=4
978 trees. Significant differences were detected by two-tailed t-test with an FDR of <0.5. * = p<0.05,
979 ** p<0.01, *** p<0.001.

980

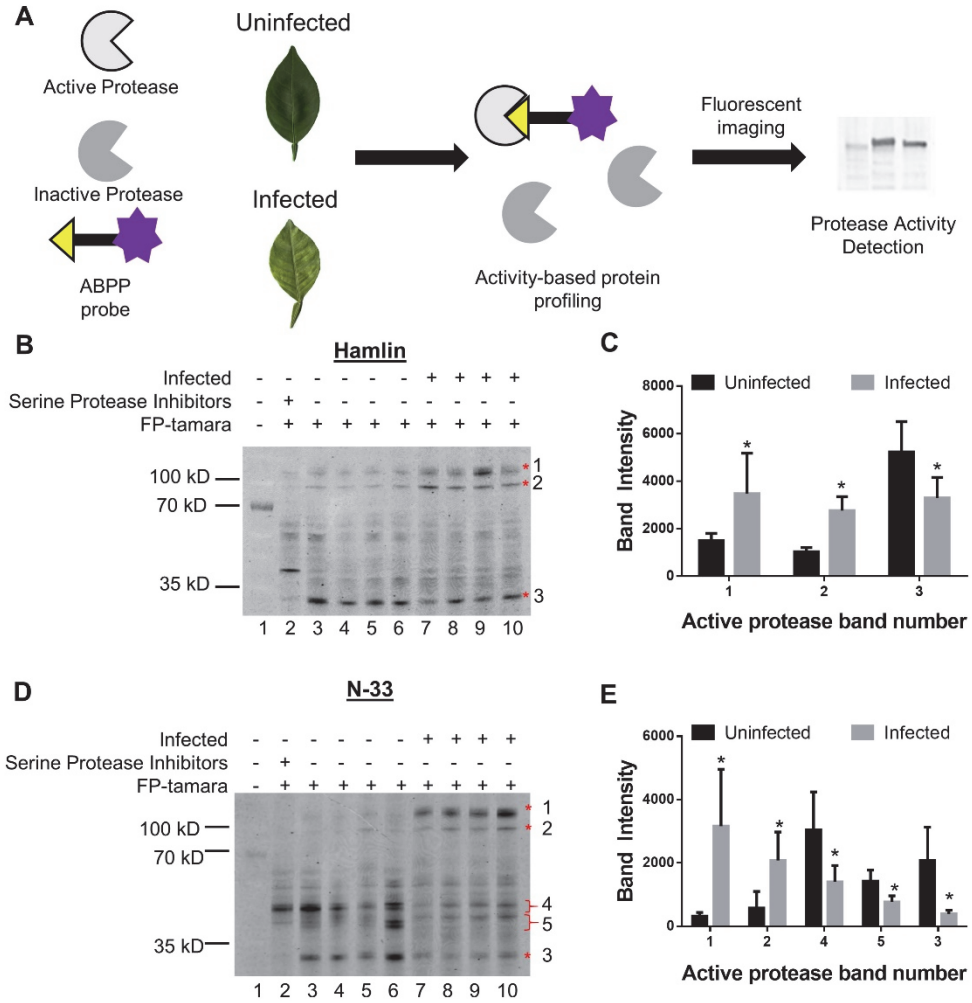

Fig 6. The activity of serine proteases dynamically changes during *C*Las infection. (A) Experimental Strategy. Proteases from uninfected and infected citrus trees were extracted and subjected to activity-based protein profiling (ABPP) using the fluorescently labeled probe, ActivX TAMRA fluorophosphonate (FP) serine hydrolase probe, to capture serine proteases. Visualization of active serine protease bands was performed with the Typhoon 8500 scanner and signals were quantified in Image J. Two sweet orange genotypes were inoculated with *C*Las using *Diaphorina citri* and analyzed for serine protease enzymatic activity. **(B)** ABPP of serine protease activity in leaves of the Hamlin variety one year after feeding with *C*Las positive and negative *D. citri.* Active serine proteases were labeled using FP-tamara (lanes 2-10). A serine protease inhibitor cocktail was pre-incubated 30 min prior to the addition of FP-tamara to demonstrate probe binding specificity (lane 2 compared to lane 3). A no probe control was added

993 as a negative control (lane 1, band is the 70kD marker from the protein ladder). Fluorescent
994 signals corresponding to serine protease activity are indicated on the right with an asterisk. **(C)**
995 Quantification of labeled band intensity in (B) using ImageJ. Graphs indicate means ±SD, n=4
996 trees. Significant differences were detected by two-tailed t-test, * = alpha-value of 0.5. **(D)** ABPP
997 of serine protease activity in leaves of the N-33 variety grown under field conditions. Gel loading
998 is the same as described in (B). Signals corresponding to active serine proteases are indicated by
999 an asterisk. Signals unable to be resolved were grouped together and indicated by brackets. **(E)**
1000 Quantification of labeled signal intensity in (C) using ImageJ. Graphs indicate means ±SD, n=4
1001 trees. Significant differences were detected by two-tailed t-test, * = alpha-value of 0.05